CUTS RNA Biosensor for the Real-Time Detection of TDP-43 Loss-of-Function

Longxin Xie*[1,2,3], Jessica Merjane*[1,3], Cristian A Bergmann*[1,3], Jiazhen Xu[1,3,4], Shruthi Balasubramaniyan[5,9], Bryan Hurtle[1,3,6], Charleen T Chu[4-8] , Christopher J Donnelly[1,3-4,6-8]

[1]Department of Neurobiology, University of Pittsburgh School of Medicine, Pittsburgh, PA, USA

[2]School of Medicine, Tsinghua University, China

[3]LiveLikeLou Center for ALS Research, University of Pittsburgh School of Medicine, Pittsburgh, PA, USA

[4]Interdisciplinary Biomedical Graduate Program Cellular and Molecular Pathology, University of Pittsburgh, Pittsburgh, PA, USA

[5]Department of Pathology, University of Pittsburgh School of Medicine, Pittsburgh, PA, USA

[6] Center for Neuroscience at the University of Pittsburgh, Pittsburgh, PA, USA

[7]Pittsburgh Institute for Neurodegeneration, University of Pittsburgh, Pittsburgh, PA, USA

[8]Center for Protein Conformational Diseases, University of Pittsburgh, Pittsburgh, PA, USA

[9] Department of Human Genetics, University of Pittsburgh School of Public Health, PA, USA

* Authors share equal contributions

Highlights

- CUTS is a cryptic exon RNA biosensor enabling real-time detection of TDP-43 loss of splicing function.
- CUTS exhibits a linear relationship with a reduction in TDP-43 protein.
- CUTS can deliver an autoregulated gene payload in response to TDP-43 loss-of-function.
- TDP-43 homotypic phase transitions and cell stress induce loss of splicing function detected via CUTS.

Abstract

Mounting evidence implicates TDP-43 dysfunction and the accumulation of pathological cryptic exons across multiple neurodegenerative diseases, underscoring the need for accessible tools to detect and quantify TDP-43 loss-of-function (LOF). These tools are crucial for assessing potential disease contributors and exploring therapeutic candidates in TDP-43 proteinopathies. Here, we

develop a sensitive and accurate real-time sensor for TDP-43 LOF: the CUTS (CFTR UNC13A TDP-43 Loss-of-Function) system. This system combines UG-rich sequences and previously reported cryptic exons regulated by TDP-43 with a reporter, enabling the tracking of TDP-43 LOF through live microscopy and RNA/protein-based assays. We show that CUTS effectively detects TDP-43 loss of function arising from mislocalization, impaired RNA binding, and pathological aggregation. Our results show the sensitivity and accuracy of the CUTS system in detecting and quantifying TDP-43 LOF, opening avenues to explore unknown TDP-43 interactions that regulate its function. In addition, by replacing the fluorescent tag in the CUTS system with the coding sequence for TDP-43, we show significant recovery of its function under TDP-43 LOF conditions, highlighting the potential utility of CUTS for self-regulating gene therapy applications. In summary, CUTS represents a platform for evaluating TDP-43 LOF in real-time and gene-replacement therapies in neurodegenerative diseases associated with TDP-43 dysfunction.

Introduction

Amyotrophic lateral sclerosis (ALS) is a progressive and fatal neurodegenerative disease (NND) characterized by a persistent degeneration of the neurons of the spinal cord and motor cortex (Feldman et al., 2022). The dysregulation of the RNA binding protein (RBP), TAR DNA-binding protein 43 (TDP-43) is a hallmark pathobiology observed in ~97% of all ALS patients (Neumann et al., 2006), ~45% of Frontotemporal lobar degeneration (FTLD) patients (Ling et al., 2013; Neumann et al., 2006), and 40%-60% of Limbic Associated TDP-43 Encephalopathy (LATE) patients (McKee et al., 2010; Nelson et al., 2019; Tremblay et al., 2011). Under physiological conditions, TDP-43 orchestrates many cellular processes critical for neuronal health and homeostasis, including regulating RNA metabolism, splicing, and stress response pathways. However, in disease, TDP-43 is depleted from the nucleus and mislocalizes to the cytoplasmic compartment, losing the ability to perform its canonical splicing function and may transition into insoluble aggregates (Hurtle et al., 2023; Mann and Donnelly, 2021).

Recent efforts increasingly focus on the implications of TDP-43's loss of splicing function and its consequence on disease onset and progression (Brown et al., 2022; Buratti and Baralle, 2001; Klim et al., 2019; Ling et al., 2015; Ma et al., 2022; Melamed et al., 2019). Physiologically, TDP-43 selectively binds to specific UG-rich sequences within pre-mRNA transcripts, providing precise control over the alternative splicing of a subset of conserved targets, thereby modulating their gene expression and cellular function (Kuo et al., 2009; Lukavsky et al., 2013). This

regulatory function is key in repressing the incorporation of TDP-43-mediated aberrant 'cryptic exons' (CE), non-conserved intronic regions whose inclusion has been linked to cellular toxicity and pathological consequences (Brown et al., 2022; Klim et al., 2019; Ling et al., 2015; Ma et al., 2022; Mehta et al., 2023; Melamed et al., 2019; Polymenidou et al., 2011). Noteworthy examples of transcripts susceptible to aberrant CEs in the absence of functional TDP-43 include *STMN2* (Klim et al., 2019; Melamed et al., 2019) and *UNC13A* (Brown et al., 2022; Ma et al., 2022), both pivotal in maintaining the integrity and physiological function of neurons, such as axon regeneration and motor neuron firing (Shin et al., 2014, 2012; Varoqueaux et al., 2002; Willemse et al., 2023). Therefore, their aberrant splicing patterns and loss-of-function (LOF) in disease highlights the critical role of TDP-43 in preserving neuronal health and function through the regulation of key neuronal health.

A well-established and currently available method to accurately monitor and quantify TDP-43's splicing function has frequently relied on employing cryptic exon 9 inclusion in the human cystic fibrosis transmembrane conductance regulator (CFTR) transgene (Buratti et al. 2001; Ayala et al. 2006). However, this approach can only be used at the RNA level, limiting its functionality as a reporting system for high-throughput screens or *in vivo* applications. Furthermore, endogenous cryptic exons exhibit variable responses to TDP-43 loss, may be cell type-specific, and are still being defined. To address this, we designed a screening tool, the 'CFTR-UNC13A TDP-43 loss-of-function Sensor' (CUTS) system, engineered to detect TDP-43 LOF and output a proportional and quantifiable signal using GFP or other reporters. By combining previously described TDP-43 binding targets with small UG stretches, we significantly improved the sensitivity measurable in real time using standard assays. Functional TDP-43 promotes the splicing of CUTS CE, resulting in a frameshift and early stop codon that prevents GFP expression. TDP-43 LOF activates the CUTS biosensor by promoting the inclusion of the CE, allowing GFP to be expressed. Here, we highlight the CUTS system sensitivity in response to TDP-43 loss. The CUTS design enables GFP expression to be directly proportional to TDP-43 LOF, allowing the detection of changes in TDP-43 function even when alterations cannot be measured directly by traditional methods like qPCR, western blot, or immunofluorescent imaging.

In this study, we highlight the utility and sensitivity of the CUTS biosensor in non-neuronal and neuronal cells. We also show that aberrant TDP-43 phase transitions or mislocalization disrupt TDP-43 splicing function by expressing well-established RNA-binding-deficient and cytoplasmic TDP-43 constructs. We also replaced the GFP cassette in the CUTS biosensor with the wild-type *TARDBP* coding sequence (CUTS-TDP43), demonstrating that CUTS can regulate a gene

payload expression in response to TDP-43 loss-of-function. The CUTS biosensor provides a sensitive and reliable means to dynamically monitor TDP-43 function and can be applied for therapeutic screening, assessment of disease-associated dysfunction, and delivery of genetic payloads in response to TDP-43 loss.

Results

CUTS TDP-43 LOF sensor design utilizing known Cryptic Exons

To improve the detection of TDP-43 LOF, we designed a novel TDP-43 LOF sensor (TS) using previously reported genes known to undergo TDP-43-regulated splicing (*UNC13A* and *CFTR*). The TS cassettes are constructed with a constitutively expressed mCherry, followed by a TDP-43-regulated CE and a GFP linked to a 3x nuclear localization signal (NLS), each separated by a T2A self-cleavage sequence (Figure 1A). We positioned the GFP reporter outside the mCherry open reading frame (ORF), introducing an early stop codon upstream of the GFP (Figure 1A). This strategic design achieved two key outcomes: (1) Under physiological TDP-43 levels, the binding of TDP-43 to the CE and UG-rich sequence should promote complete intronic splicing, maintaining the in-frame stop codon upstream of GFP, resulting in only mCherry expression. (2) TDP-43 loss and/or failure to bind the CE sites will result in CE retention and a subsequent frameshift that bypasses the stop codon, allowing translation to proceed into the GFP coding sequence, leading to co-expression of mCherry and GFP. This system will allow a systematic screen of whether any TDP-43 perturbation is causing LOF, which should be proportional to GFP signal output.

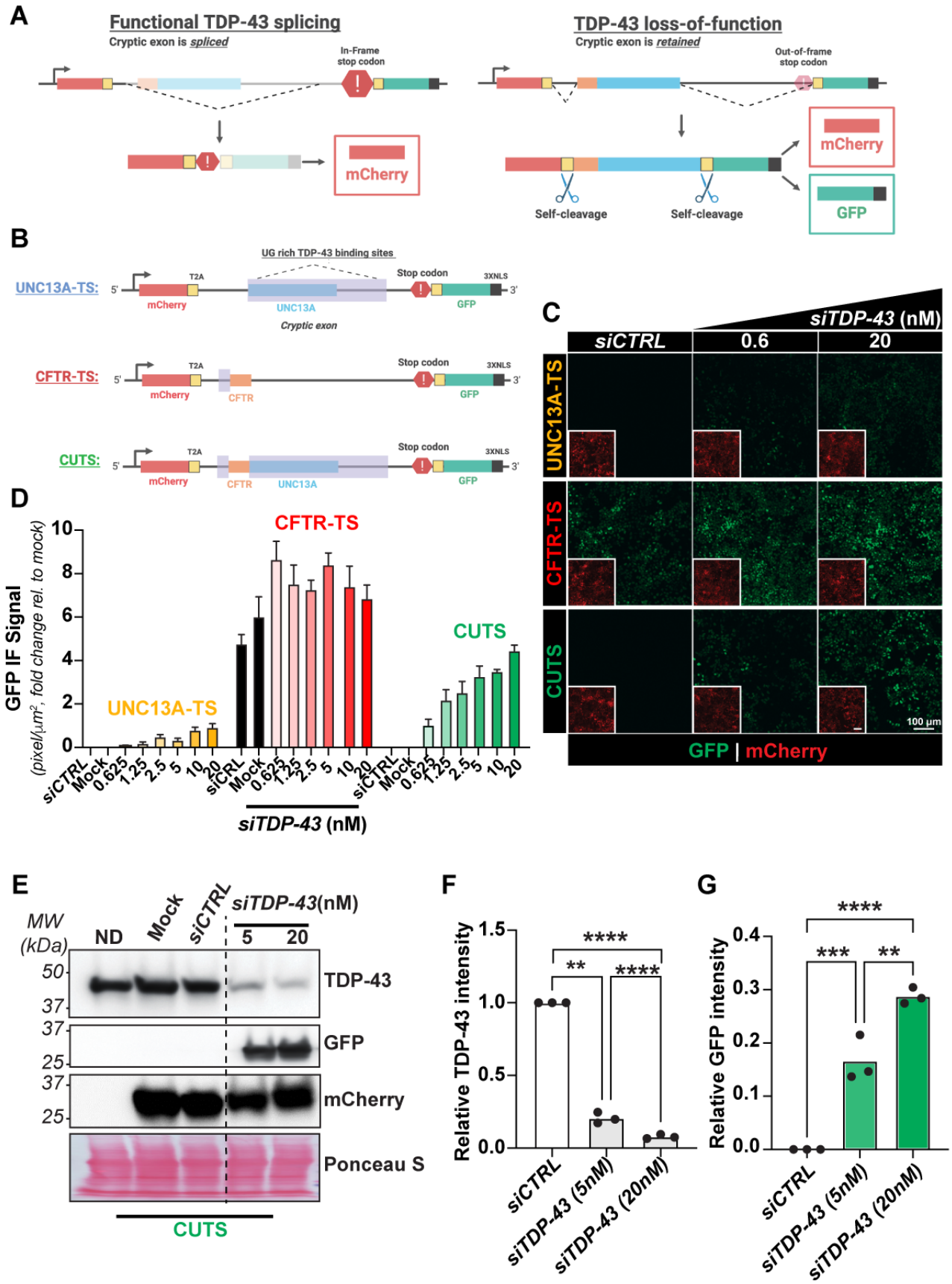
A
Functional TDP-43 splicing
Cryptic exon is spliced
In-Frame stop codon
mCherry
TDP-43 loss-of-function
Cryptic exon is retained
Out-of-frame stop codon
mCherry
GFP
Self-cleavage
Self-cleavage
B
UG rich TDP-43 binding sites
UNC13A-TS:
T2A
Stop codon
3XNLS
mCherry
UNC13A
GFP
Cryptic exon
CFTR-TS:
CFTR
CUTS:
C
siTDP-43 (nM)
siCTRL
0.6
20
UNC13A-TS
CFTR-TS
CUTS
100 µm
GFP | mCherry
D
GFP IF Signal
(pixel/µm², fold change rel. to mock)
CFTR-TS
CUTS
UNC13A-TS
siCTRL
Mock
0.625
1.25
2.5
5
10
20
siTDP-43 (nM)
E
MW (kDa)
ND
Mock
siCTRL
siTDP-43(nM)
5
20
TDP-43
GFP
mCherry
Ponceau S
CUTS
F
Relative TDP-43 intensity
siCTRL
siTDP-43 (5nM)
siTDP-43 (20nM)
G
Relative GFP intensity
siCTRL
siTDP-43 (5nM)
siTDP-43 (20nM)

116

117 ***Figure 1: Design and functional comparison of TDP-43 loss-of-function reporter systems.***
118 *Comparison of stable polyclonal HEK cells expressing UNC13A-TS, CFTR-TS, or CUTS following*
119 *treatment with siRNA control (siCTRL) (20nM) or TDP-43 (siTDP-43) (0.6nM - 20nM). Cells were*
120 *reverse-transfected with siRNA treatment in complete media supplemented with doxycycline*
121 *(1000 ng/mL). As a negative control, we use ND: No doxycycline. After 72 h, cells were analyzed*
122 *by live imaging and protein lysate was harvested for western blot analysis.* ***(A)*** *Schematic of the*
123 *TDP-43 loss-of-function Sensor (TS) system design.* ***(B)*** *Overview of the UNC13A-TS, CFTR-TS,*
124 *and CUTS cryptic exon cassette design.* ***(C)*** *Representative live imaging of TS comparison (10X)*
125 *nuclear GFP indicates TDP-43 LOF.* ***(D)*** *Mean intensity quantification of GFP signal intensity as*
126 *shown in (C).* ***(E)*** *Western blot analysis of CUTS immunoblotting for TDP-43 and GFP proteins.*
127 ***(F-G)*** *Relative pixel quantification of TDP-43 and GFP band normalized to total protein (Ponceau*
128 *S) from (E). Statistical significance was determined by one-way ANOVA and Tukey's multiple*
129 *comparison test (*, $p < 0.05$; **, $p < 0.01$; ***, $p < 0.001$; ****, $p < 0.0001$). Green = GFP signal;*
130 *red = mCherry signal. Scale bar = 100 µm. N=3 biological replicates.*

1

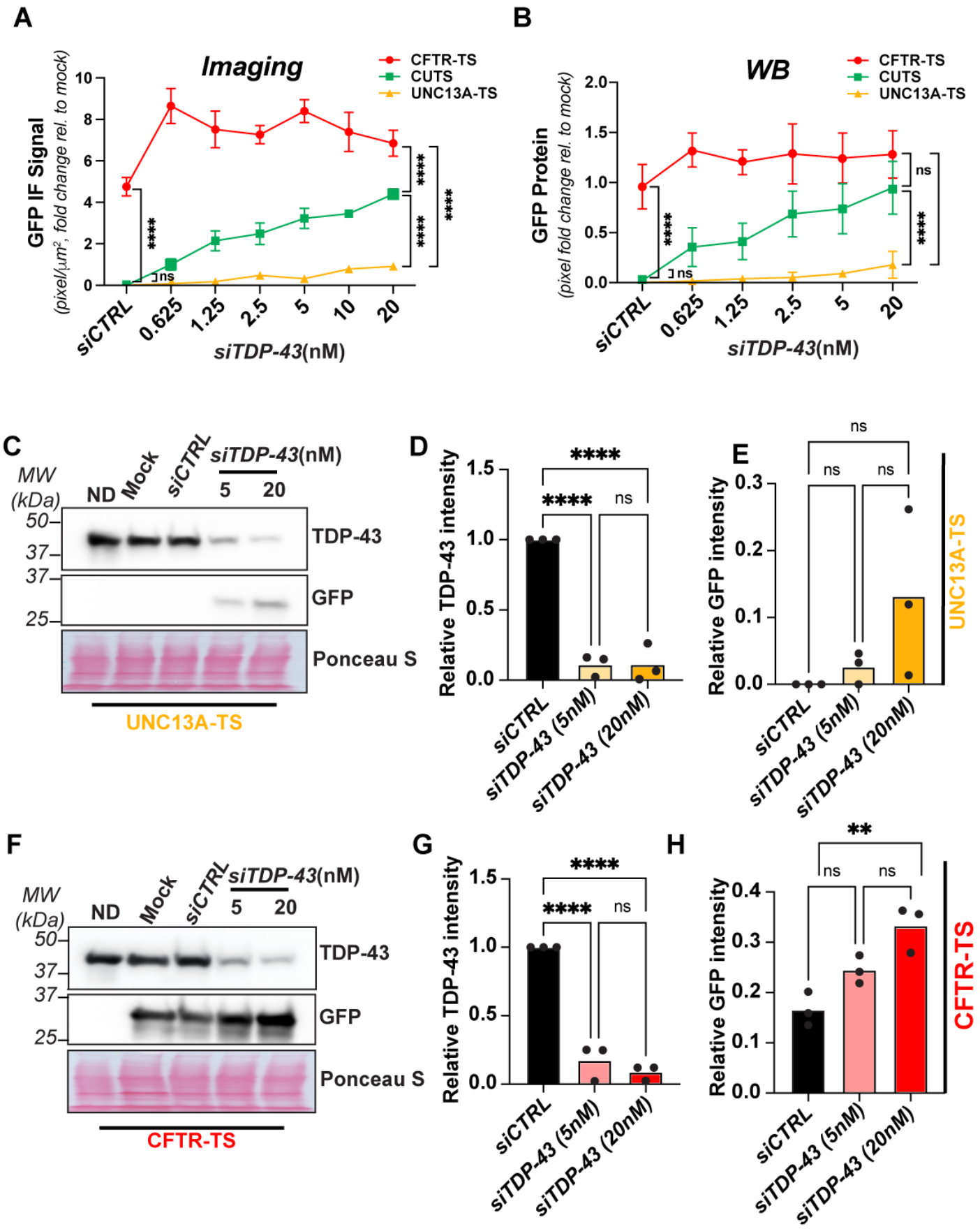
A
Imaging
CFTR-TS
CUTS
UNC13A-TS
GFP IF Signal
(pixel/μm², fold change rel. to mock)
siCTRL
0.625
1.25
2.5
5
10
20
siTDP-43(nM)
****
ns
B
WB
GFP Protein
(pixel fold change rel. to mock)
C
MW (kDa)
ND
Mock
siCTRL
siTDP-43(nM)
5
20
TDP-43
GFP
Ponceau S
UNC13A-TS
D
Relative TDP-43 intensity
siCTRL
siTDP-43 (5nM)
siTDP-43 (20nM)
E
Relative GFP intensity
UNC13A-TS
F
CFTR-TS
G
H
**
CFTR-TS

132 ***Supplementary Figure 1: Differential reporter sensitivity to TDP-43 depletion.*** *Comparison*
133 *of stable polyclonal HEK cells expressing UNC13A-TS, CFTR-TS, or CUTS following treatment*
134 *with siRNA control (siCTRL) (20nM) or TDP-43 (siTDP-43) (0.6nM - 20nM). Cells were reverse-*
135 *transfected with siRNA treatment in complete media supplemented with doxycycline (1000 ng/mL).*
136 *After 72 h, cells were analyzed by live imaging and protein lysate was harvested for western blot*
137 *analysis. (**A)** Mean intensity quantification of GFP signal intensity from live imaging, presented as*
138 *fold change from mock. **(B)** Relative pixel quantification of GFP normalized to total protein*
139 *(Ponceau S), presented as fold change from mock. **(C-E)** WB analysis of UNC13A-TS, developing*
140 *again TDP-43 and GFP proteins, and pixel quantification of TDP-43 and GFP intensity from bands*
141 *show in (C) normalized to total protein (Ponceau S). **(F-H)** WB analysis of CFTR-TS, developing*
142 *again TDP-43 and GFP proteins, and pixel quantification of TDP-43 and GFP intensity from bands*
143 *show in (F) normalized to total protein (Ponceau S). Statistical significance was determined by*
144 *two-way ANOVA and Tukey's multiple comparison test (*, $p < 0.05$; **, $p < 0.01$; ***, $p < 0.001$;*
145 *****, $p < 0.0001$). N=3 biological replicates.*

146

147 **CUTS is more precise than CFTR and UNC13A as a TDP-43 LOF biosensor**

148 To assess the functionality of TS, we engineered UNC13A-TS, CFTR-TS, and CUTS,
149 which utilized the TDP-43-regulated CEs from UNC13A, CFTR, and a combined construct termed
150 CUTS (CFTR-UNC13A TS), integrating both CE sequences (Figure 1B). Additional base
151 modifications were incorporated into the cassette designs to prevent unexpected stop codons
152 within the CE regions (see Table S1 for full sequence details). Each construct was coupled with
153 a Tet3g promoter, cloned into a Piggybac vector, and stably expressed in HEK293 cells. To
154 evaluate the accuracy and reliability of the three TS constructs, we performed a TDP-43 LOF
155 assay using increasing *siRNA* concentrations, followed by live confocal imaging and western blot
156 (WB) analysis (Figure 1C-G and S1A-H). Across all cell lines, we observed constitutive mCherry
157 expression and a trend toward increased GFP signals with higher *siTDP-43* concentrations. The
158 UNC13A-TS construct demonstrated no detectable GFP expression under control conditions in
159 both imaging-based and WB analyses (Figure 1 C-D, S1A-E). However, the UNC13A-TS showed
160 limited sensitivity, with only a modest GFP signal (17% of CUTS) detected via imaging under the
161 highest dose of siTDP-43 treatment assessed (20nM; Figure 1D). In contrast, the CFTR-TS
162 construct exhibited a notably high baseline, with detectable GFP leakage in control groups without
163 TDP-43 loss (Figure 1C-D, S1A-B, F-H). Interestingly, cells expressing the CUTS construct
164 exhibited a synergistic effect from both the CFTR and UNC13A CE sequences, achieving high

sensitivity evidenced by a clear dose-responsive GFP expression with increasing siTDP-43 concentrations, while maintaining high accuracy with minimal leakage via imaging and GFP immunoblotting (Figure 1C-G). Given the promising accuracy of the CUTS sensor, we proceeded to further characterize the CUTS RNA biosensor.

CUTS demonstrates ultra-sensitivity in detecting low-level TDP-43 loss-of-function

To challenge the stability and sensitivity of CUTS, we next conducted an ultra-low dose TDP-43 *siRNA* transfection, ranging from 38-1200 pM. Immunofluorescence staining (IF) revealed a consistent increase in both GFP intensity and GFP-positive cell ratios in CUTS-expressing cells in response to elevated *siTDP-43*, with minimal baseline expression observed (Figure 2A-B). We confirmed the ultra-sensitivity and accuracy of CUTS using WB analysis, demonstrating measurable GFP even at the lowest doses of *siTDP-43* assessed (Figure 1C-E). While changes in TDP-43 levels were undetectable by WB at *siTDP-43* doses of 37.5-75 pM (measured as 2% TDP-43 KD by WB, see Figure S2A), the CUTS system demonstrated a 7 to 55-fold increase in GFP expression at these doses compared to baseline (Figure S2A). This increase in GFP expression persisted to the highest siTDP-43 dose (1,200 pM; 98% TDP-43 KD; Figure S2A), resulting in a 118,224-fold increase in GFP compared to baseline. Pearson's correlation analysis confirmed a highly significant relationship between GFP expression and siTDP-43 dose (p=0.0011), while the correlation between measurable TDP-43 and siTDP-43 concentration was less significant (p=0.0429) (Figure 2D-E). Linear regression analysis between the logarithmic GFP fold increase and siRNA doses demonstrated an exceptional linear relationship (R^2=0.9998) (Figure 2E). These results indicate that GFP expression produced by CUTS is a more sensitive method for detecting TDP-43 KD (and therefore LOF) than TDP-43 WB detection. The linear relationship between GFP and siTDP-43 dose also demonstrates the potential of CUTS to be used as a predictive model for TDP-43 LOF.

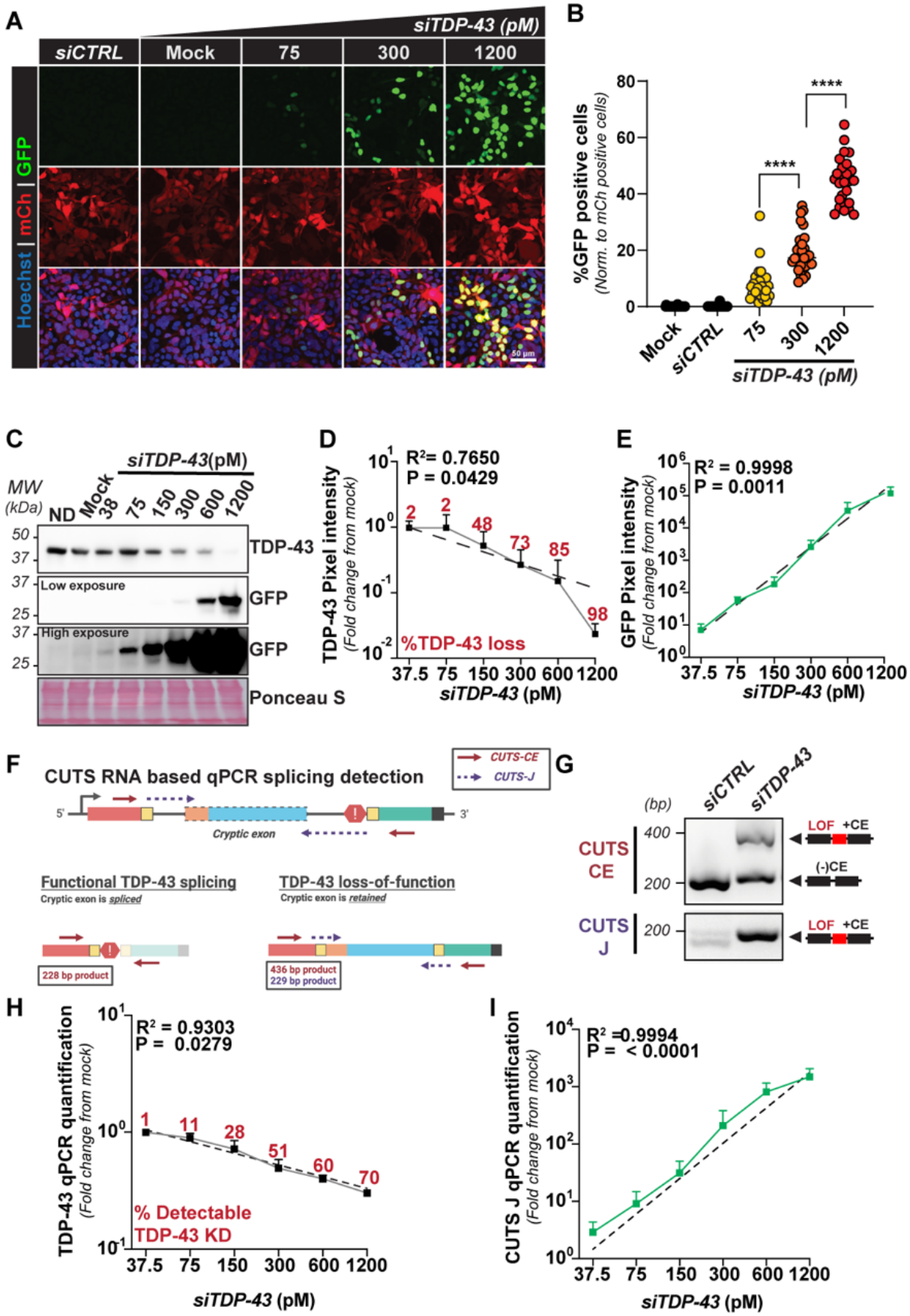
A
siTDP-43 (pM)
siCTRL
Mock
75
300
1200
Hoechst | mCh | GFP
50 µm
B
%GFP positive cells
(Norm. to mCh positive cells)
****
****
Mock
siCTRL
siTDP-43 (pM)
C
siTDP-43(pM)
MW (kDa)
ND
Mock
38
75
150
300
600
1200
TDP-43
Low exposure
GFP
High exposure
GFP
Ponceau S
D
R²= 0.7650
P = 0.0429
TDP-43 Pixel intensity
(Fold change from mock)
%TDP-43 loss
siTDP-43 (pM)
E
R² = 0.9998
P = 0.0011
GFP Pixel intensity
(Fold change from mock)
siTDP-43 (pM)
F
CUTS RNA based qPCR splicing detection
CUTS-CE
CUTS-J
Cryptic exon
Functional TDP-43 splicing
Cryptic exon is spliced
TDP-43 loss-of-function
Cryptic exon is retained
228 bp product
436 bp product
229 bp product
G
siCTRL
siTDP-43
(bp)
CUTS CE
CUTS J
LOF +CE
(-)CE
H
R² = 0.9303
P = 0.0279
TDP-43 qPCR quantification
(Fold change from mock)
% Detectable TDP-43 KD
siTDP-43 (pM)
I
R² =0.9994
P = < 0.0001
CUTS J qPCR quantification
(Fold change from mock)
siTDP-43 (pM)

190

Figure 2: CUTS exhibits linear, dose-responsive activation following low-level TDP-43 knockdown. *Low-dose siRNA TDP-43 (siTDP-43) treatment was performed in stable polyclonal HEK cells expressing CUTS. CUTS-expressing cells were reverse transfected with siRNA control (siCTRL) or siTDP-43 in a dose-response curve (38 to 1200pM) in doxycycline supplemented media (1000ng/ml) for 72hr.* ***(A)*** *Representative immunofluorescence images of CUTS-expressing HEK cells under low doses of siRNA TDP-43 treatment. (60X).* ***(B)*** *Percentage of GFP-positive cells normalized to the number of CUTS-expressing mCherry-positive cells.* ***(C)*** *Western blot of TDP-43 and GFP proteins from HEK cell lysate expressing CUTS under low doses of siRNA TDP-43. Ponceau S is shown as a loading control.* ***(D)*** *Pixel intensity quantification of the TDP-43 and* ***(E)*** *GFP bands shown in (C), presented as fold-change from the mock-treated sample.* ***(F)*** *Schematic showing the position of qPCR primers, developed to detect CUTS cryptic exon inclusion (referred to as 'CUTS-CE' and 'CUTS-J').* ***(G)*** *Representative agarose gel showing qPCR product from melting curve detecting CUTS cryptic exon inclusion using the primers shown in (F).* ***(H-I)*** *qPCR quantification of TDP-43 and CUTS cryptic exon J from the siTDP-43 dose curve presented as fold-change from the mock-treated sample. Linear regression analysis shown in (D), (E), (H) and (I) was performed on Log values. Fitting method = least squares regression. (****, $p < 0.0001$). N=3 biological replicates. Green = GFP; red = mCherry. Scale bar = 50 µm. N=3 biological replicates.*

We assessed CUTS' sensitivity at the transcript level using the *siTDP-43* ultra-low dose curve and RT-qPCR assessment in Figure 2F-I. To determine the relative amount of CUTS' CE retention, we designed primers targeting either the entire transcript or the specific junction sites of the CE (Figure 2F-G). The RT-qPCR quantification demonstrated increased sensitivity at detecting changes in TDP-43 levels compared to WB analysis, with the capability of detecting changes in TDP-43 between each siTDP-43 dose (1 – 70% TDP-43 KD, see Figure 2H and Figure S2B) in a linear manner (R^2 = 0.9303). Using CUTS detection, we observed a clear linear logarithmic relationship between the amount of CUTS CE-retention and the increasing *siTDP-43* doses (R^2=0.9994) (Figure 2I and Figure 2SB). Even at 1% KD in TDP-43, the CUTS system detected a 3-fold increase in CE retention compared to baseline, which increased to a 1,488-fold increase at 70% TDP-43 KD (Figure 2I and Figure 2SB). As with our WB analysis (Figure 2D), there was a significant correlation between GFP expression and TDP-43 and the siTDP-43 dose ($p < 0.0001$ and $p = 0.0279$, respectively). Thus, this data suggests that CUTS is a reliable tool to quantify

223 TDP-43's function across an extensive functional range, highlighting its utility as a TDP-43 LOF
224 biosensor.

225 Additionally, CUTS demonstrated ultra-sensitivity under low-level TDP-43 KD, beyond the
226 detection limit of both WB and RT-qPCR. We next sought to compare the ultra-sensitive detection
227 capacity of the CUTS sensor with the physiological response of CEs inclusion on genes regulated
228 by TDP-43 (Figure S2E). Using low concentrations of siTDP-43, we were able to recapitulate
229 CUTS sensitivity to detect CE inclusion at low-dose siRNA (75 pM) by RT-PCR. Interestingly,
230 LPR8, ARHGAP32, and ACBD3 CEs displayed a similar pattern, showing progressive CE
231 inclusion with increasing *siTDP-43* doses, starting at 75 pM. However, HDGFL2 showed higher
232 sensitivity to TDP-43 LOF, with detectable exon inclusion even at 38 pM (Figure 2SE). Together,
233 these results establish CUTS as a relevant tool to evaluate sensitively and quantitatively minimal
234 reductions in TDP-43 levels and accurately report its LOF.

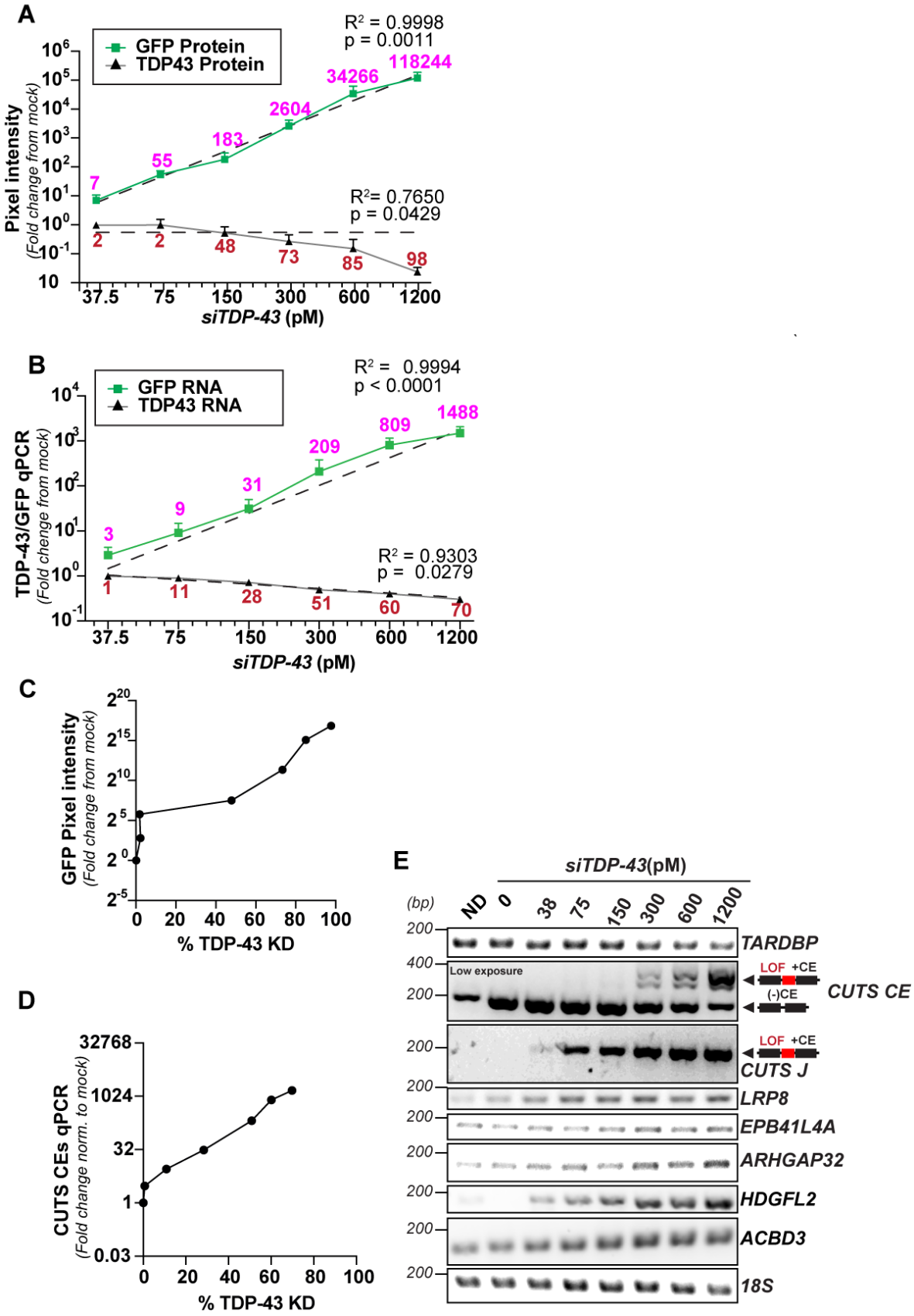
A
GFP Protein
TDP43 Protein
R² = 0.9998
p = 0.0011
R²= 0.7650
p = 0.0429
Pixel intensity
(Fold change from mock)
siTDP-43 (pM)
B
GFP RNA
TDP43 RNA
R² = 0.9994
p < 0.0001
R² = 0.9303
p = 0.0279
TDP-43/GFP qPCR
(Fold chenge from mock)
siTDP-43 (pM)
C
GFP Pixel intensity
(Fold change from mock)
% TDP-43 KD
D
CUTS CEs qPCR
(Fold change norm. to mock)
% TDP-43 KD
E
siTDP-43(pM)
ND
0
38
75
150
300
600
1200
(bp)
TARDBP
Low exposure
LOF
+CE
(-)CE
CUTS CE
CUTS J
LRP8
EPB41L4A
ARHGAP32
HDGFL2
ACBD3
18S

235

236 **Supplementary Figure 2: CUTS signal scales with dose-dependent TDP-43 knockdown.**
237 *Low-dose siTDP-43 treatment was performed in stable polyclonal HEK cells expressing CUTS.*
238 *CUTS-expressing cells were reverse transfected with siCTRL or siTDP43 in a dose-response*
239 *curve (38 - 1200 pM) in doxycycline supplemented media (1000ng/ml) for 72 h.* ***(A)*** *Pixel*
240 *intensity quantification of the GFP and TDP-43 bands shown in (C), presented as fold-change*
241 *from the mock-treated sample.* ***(B)*** *qPCR quantification of the siTDP-43 dose curve presented*
242 *as fold-change from the mock-treated sample. Purple text above indicates the GFP fold change*
243 *from the mock-treated sample. Red text above indicates the percentage of total detectable TDP-*
244 *43 knockdown. Linear regression analysis shown in (D) and (G) was performed on Log values.*
245 *Fitting method = least squares regression.* ***(C)*** *GFP pixel intensity from the Western blot shown*
246 *in Figure 2C plotted against the percentage of TDP-43 knockdown detected under siTDP-43*
247 *treatment (38 -1200 pM).* ***(D)*** *CUTS CE transcript quantification plotted against the percentage*
248 *of TDP-43 knockdown detected under siTDP-43 treatment (38 - 1200 pM).* ***(E)*** *RT-PCR of*
249 *endogenous cryptic exons and the CUTS biosensor following increasing doses of siTDP43*
250 *treatment.*

251 **Pathological TDP-43 phase transitions or mislocalization activate the CUTS biosensor**

252 In ALS/FTLD, the absolute TDP-43 level remains largely unaffected. Instead, TDP-43
253 undergoes pathological mislocalization and/or phase transitions likely due to a reduction in RNA
254 binding, which reduces the functional cellular TDP-43. To evaluate whether these events
255 contribute to TDP-43 LOF, we tested CUTS's ability to detect TDP-43 LOF caused by TDP-43
256 mislocalization or aggregation via aberrant phase transitions. We transfected CUTS HEK293 cells
257 with four tagged TDP-43 isoforms: (1) TDP-43^{WT}, (2) TDP-43^{cyto}, (3) TDP-43^{5FL}, and (4) TDP-43^{cyto}
258 ^{5FL}. The TDP-43^{cyto} variants contain point mutations located within the nuclear localization signal
259 (NLS) of TDP-43, resulting in cytoplasmic mislocalization (Mann et al., 2019). The 5FL form
260 contains five phenylalanine-to-leucine mutations within the two RNA recognition motif (RRM)
261 domains of TDP-43 that greatly impaired TDP-43's RNA binding ability and were previously
262 reported to form aggregated "anisomes" inside the nucleus (Cohen et al., 2015; Elden et al.,
263 2010; Mann et al., 2019; Yu et al., 2021). The TDP-43$^{cyto\ 5FL}$ combines both modifications, leading
264 to insoluble cytoplasmic inclusions (Elden et al., 2010; Keating et al., 2023; Lu et al., 2022; Mann
265 et al., 2019; Yu et al., 2021). Excluding TDP-43^{WT}, all three modified versions have been proven
266 to sequestrate endogenous TDP-43 into mislocalized or aggregated inclusions (Keating et al.,
267 2023). Therefore, our objective was to utilize CUTS to determine whether the expression of these
268 aggregation-prone TDP-43 variants elicits endogenous TDP-43 LOF.

The introduction of TDP-43^{cyto}, TDP-43^{5FL}, and TDP-43$^{cyto\ 5FL}$ induced nuclear GFP signal when assessed by immunofluorescence analysis, while neither the tagged plasmid backbone nor TDP-43^{WT} caused any detectable GFP (Figure 3A). We confirmed the expression of exogenous and endogenous TDP-43 levels by WB and quantified the relative GFP level in each condition (Figure 3B-3C). As we have previously shown that CUTS demonstrates a proportional response to TDP-43's LOF (Figure 2), we were able to directly interpret the relative ability of the different TDP-43 mutants to trigger TDP-43 LOF by comparison of their GFP levels. All three TDP-43 mutants' expression triggered significant LOF compared to the control conditions, albeit at varying significance levels. The most modest LOF effect was achieved by TDP-43^{cyto}, followed by TDP-43$^{cyto\ 5FL}$, and TDP-43^{5FL} (Figure 3C). Interestingly, although both TDP-43^{5FL} and TDP-43$^{cyto\ 5FL}$ caused significantly elevated LOF, the TDP-43^{5FL} mutant alone mediated greater LOF than when combined with the NLS mutations highlighting the potential role of nuclear homotypic TDP-43 interactions potentially contributing to TDP-43 LOF in disease absent its cytoplasmic mislocalization. To further validate the functionality of exogenous TDP-43, we transfected TDP-43^{WT} into a HeLa TDP-43 knock-out cell line expressing CUTS (Roczniak-Ferguson & Ferguson, 2019). We detected a significantly decreased GFP signal compared to the backbone or non-transfected controls, which confirmed the full splicing function of TDP-43^{WT} (Figure S3A-S3D).

We next tested whether CUTS can detect TDP-43 LOF under oxidative stress induced by sodium arsenite ($NaAsO_2$), previously shown to disrupt TDP-43 splicing activity (Huang et al., 2024). CUTS showed mild activation, with detectable GFP signal and a significant increase in GFP intensity compared to mock treated cells (Figure 3D–E). While TDP-43 mRNA levels remained unchanged (Figure 3F), CUTS transcripts were markedly upregulated (Figure 3G). Consistent with this, endogenous cryptic exons ATG4B and GPSM2 were increased, whereas KCNQ2 was unaffected (Figure 3H-I)(Estades Ayuso et al., 2023; Joseph et al., 2025; Schmidt et al., 2019). These results highlight the sensitivity of CUTS in detecting subtle TDP-43 functional loss, which is often difficult to capture using an endogenous marker. Taken together, these data show the functional consequence caused by TDP-43's mislocalization and/or aberrant phase transitions, demonstrating that aggregation-prone TDP-43 variants mediated direct LOF toxicity in addition to any gain-of-function (GOF) toxic events. Furthermore, these results strongly support CUTS's ability to measure functional TDP-43 levels under cell stress and other paradigms beyond TDP-43 KD.

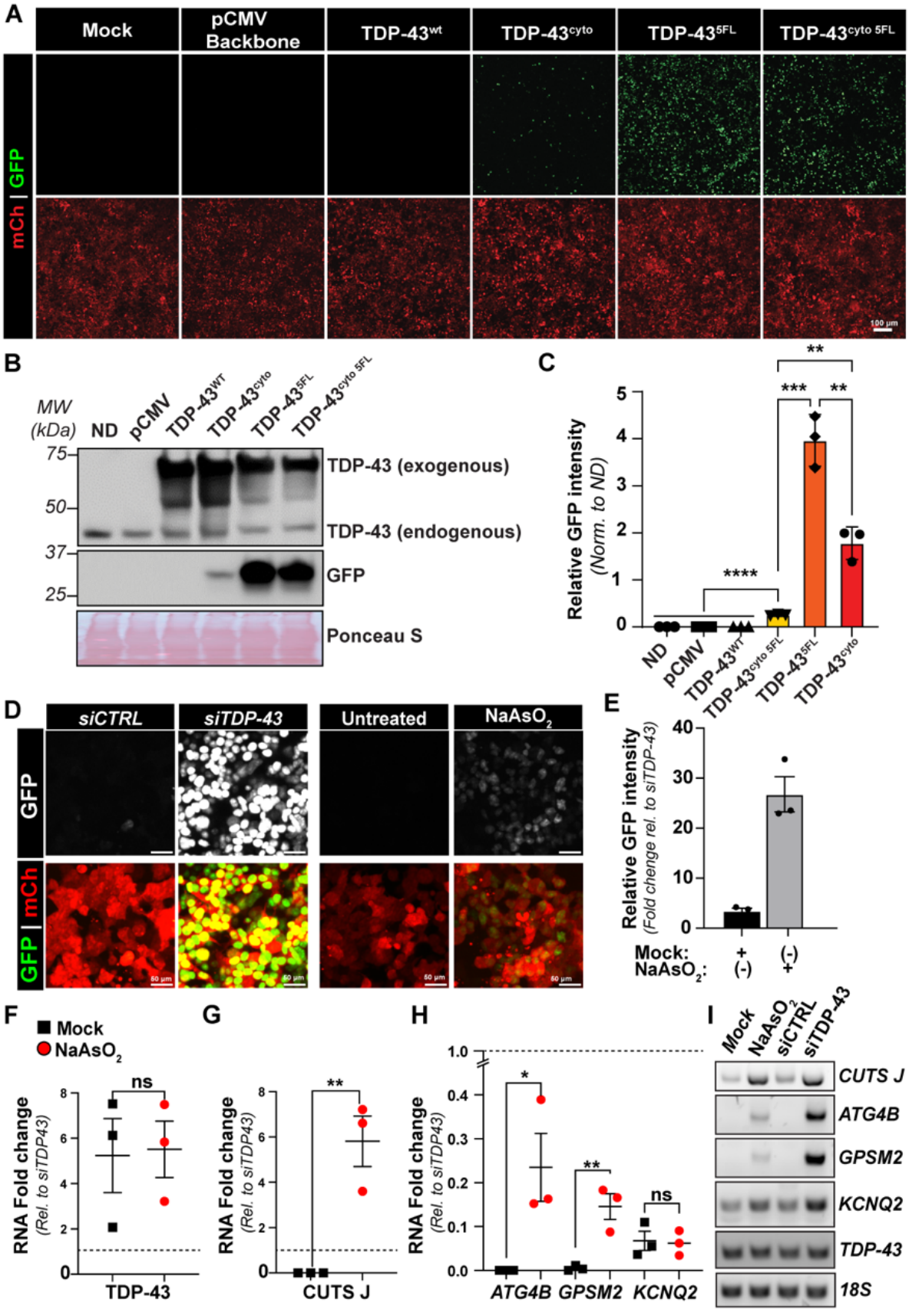
A
Mock
pCMV Backbone
TDP-43wt
TDP-43cyto
TDP-43 5FL
TDP-43cyto 5FL
GFP
mCh
100 µm
B
MW (kDa)
ND
pCMV
TDP-43WT
TDP-43cyto
TDP-43 5FL
TDP-43cyto 5FL
75
50
37
25
TDP-43 (exogenous)
TDP-43 (endogenous)
GFP
Ponceau S
C
Relative GFP intensity (Norm. to ND)
****
***
**
**
ND
pCMV
TDP-43WT
TDP-43cyto 5FL
TDP-43 5FL
TDP-43cyto
D
siCTRL
siTDP-43
Untreated
NaAsO2
GFP
GFP | mCh
50 µm
E
Relative GFP intensity (Fold chenge rel. to siTDP-43)
Mock:
NaAsO2:
F
Mock
NaAsO2
ns
RNA Fold change (Rel. to siTDP43)
TDP-43
G
**
CUTS J
H
*
**
ns
ATG4B
GPSM2
KCNQ2
I
Mock
NaAsO2
siCTRL
siTDP-43
CUTS J
ATG4B
GPSM2
KCNQ2
TDP-43
18S

300

301 ***Figure 3: Mislocalization and aberrant phase transitions induce TDP-43 LOF.***
302 *Stable HEK cells expressing CUTS were induced with doxycycline (1000 ng/mL) for 24 hours*
303 *before transfection with the following plasmids: pCMV backbone, TDP-43^{WT}, TDP-43$^{\Delta NLS}$, TDP-*
304 *43^{5FL}, TDP-43$^{\Delta NLS\ 5FL}$, or non-transfected. Following transfection, plasmids were expressed for 72*
305 *h, followed by live imaging and protein analysis.* ***(A)*** *Live-imaging of CUTS HEK cells expressing*
306 *WT or mutant TDP-43 gene cassettes.* ***(B)*** *Representative western blot of exogenous and*
307 *endogenous GFP and TDP-43. Ponceau S is shown as a loading control.* ***(C)*** *Relative GFP pixel*
308 *intensity quantification of the band is shown in (B).* ***(D–E)*** *Immunofluorescence of stable HEK*
309 *cells expressing CUTS with siCTRL (20 nM), siTDP-43 (20 nM), mock, and $NaAsO_2$ (250 μM).*
310 ***(E)*** *Immunofluorescence GFP signal quantification of (D) with 250 μM $NaAsO_2$ treatment relative*
311 *to siTDP-43 (20 nM).* ***(F-G)*** *RT-qPCR from CUTS-expressing HEK cells treated with 250 μM*
312 *$NaAsO_2$ of TDP-43, CUTS-J transcript, and endogenous cryptic exons (ATGB4, GPSM2, and*
313 *KCNQ2) relative to siRNA TDP-43 20 nM (dotted line) and normalized to 18S.* ***(I)*** *RT-PCR from*
314 *Figure F-H. Expression values were normalized to 18S rRNA, and fold changes were calculated*
315 *relative to the siTDP-43 (20 nM) condition. Black squares= Mock: Red circle= $NaAsO_2$. Statistical*
316 *significance was determined by one-way ANOVA and Tukey's multiple comparison test (*, $p <$*
317 *0.05; **. $p < 0.01$; ***. $p < 0.001$; ****, $p < 0.0001$). Green = GFP; red = mCherry. Scale bar = 100*
318 *μm. N = 3 biological replicates.*

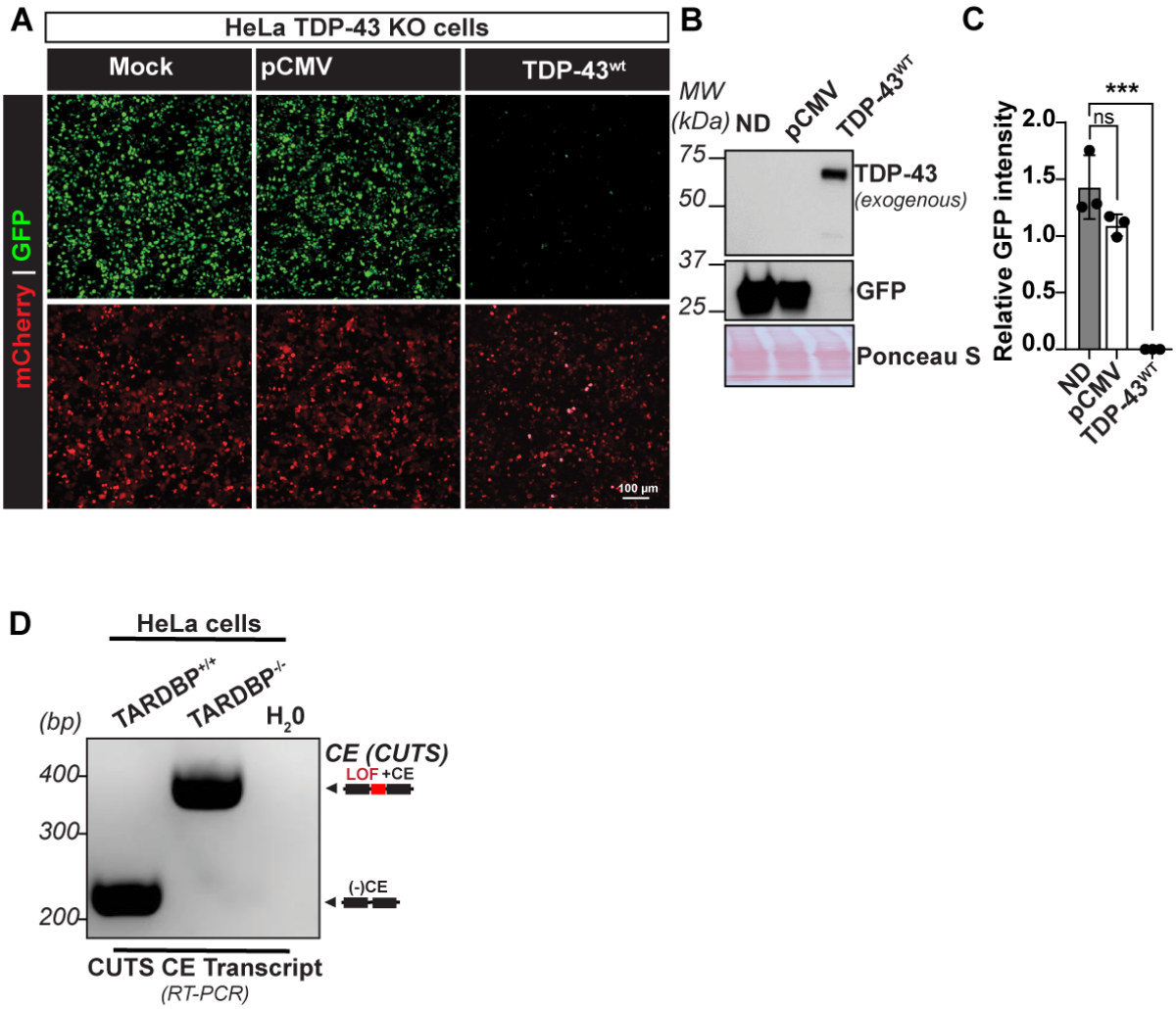

Supplementary Figure 3: TDP-43^{wt} expression rescues loss-of-function in a HeLa TARDBP Knockout Cell Line. *Transient CUTS expression in HeLa TDP-43 KO we induced with doxocycline (1000n/ml) for 24 hours before transfection of pCM backbone or TDP-43^{WT} plasmids. Following transfection, plasmids were expressed for 72 h, followed by live imaging and protein analysis.* ***(A)*** *Live-imaging of HeLa TDP-43 KO expressing CUTS in combination with TDP-43^{WT} or pCMV backbone control.* ***(B)*** *Representative WB of exogenous and endogenous GFP and TDP-43. Ponceau S is shown as a loading control.* ***(C)*** *Relative GFP pixel intensity quantification of the protein bands shown in (B).* ***(D)****RT-PCR product from CUTS cryptic exon inclusion from wildtype or TDP-43 KO HeLa cell lines using the CUTS-CE primers shown in Figure 2E. Statistical significance was determined by one-way ANOVA and Tukey's multiple comparison test (*, $p < 0.05$; **, $p < 0.01$; ***, $p < 0.001$; ****, $p < 0.0001$). Green = GFP; red = mCherry. Scale bar = 100 µm. N = 3 biological replicates.*

332 **CUTS-mediated autoregulated restoration of TDP-43 splicing.**

333 Given the growing recognition of the role TDP-43 LOF is believed to play in disease
334 progression, numerous efforts have been committed to developing rescue methods aimed at re-
335 delivering TDP-43 or other gene payloads to restore its physiological splicing function (Baughn et
336 al., 2023; Mehta et al., 2023; Sun et al., 2017). However, a significant challenge in LOF therapies
337 lies in maintaining precise TDP-43 levels within neurons, as even slight overexpression can lead
338 to GOF toxicity (Johnson et al., 2009; Park et al., 2017; Yang et al., 2022). Consequently, a
339 generalized TDP-43 gene-replacement therapy without genome integration carries a substantial
340 risk of overexpression toxicity. Therefore, a CE biosensor such as CUTS may be used to control
341 cell- and temporal-specific regulation of a gene payload. To test this, we generated a CUTS-
342 controlled TDP-43 (CUTS-TDP43) transgene (Figure 4A). Considering the ultra-sensitivity to
343 TDP-43 LOF and minimal leakage under physiological TDP-43 levels, CUTS-TDP43 may have
344 the potential to autonomously negatively regulate its expression, ensuring levels will not surpass
345 physiological levels.

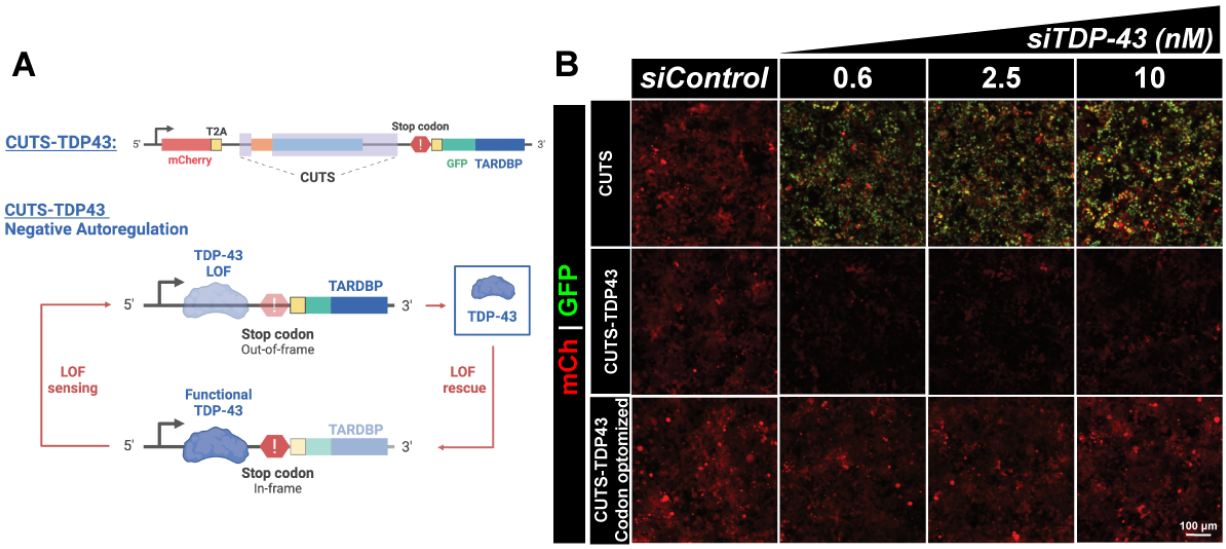
A
CUTS-TDP43:
T2A
mCherry
CUTS
Stop codon
GFP
TARDBP
CUTS-TDP43
Negative Autoregulation
TDP-43
LOF
TARDBP
Stop codon
Out-of-frame
TDP-43
LOF
sensing
LOF
rescue
Functional
TDP-43
TARDBP
Stop codon
In-frame
B
siTDP-43 (nM)
siControl
0.6
2.5
10
mCh | GFP
CUTS
CUTS-TDP43
CUTS-TDP43
Codon optomized
100 µm

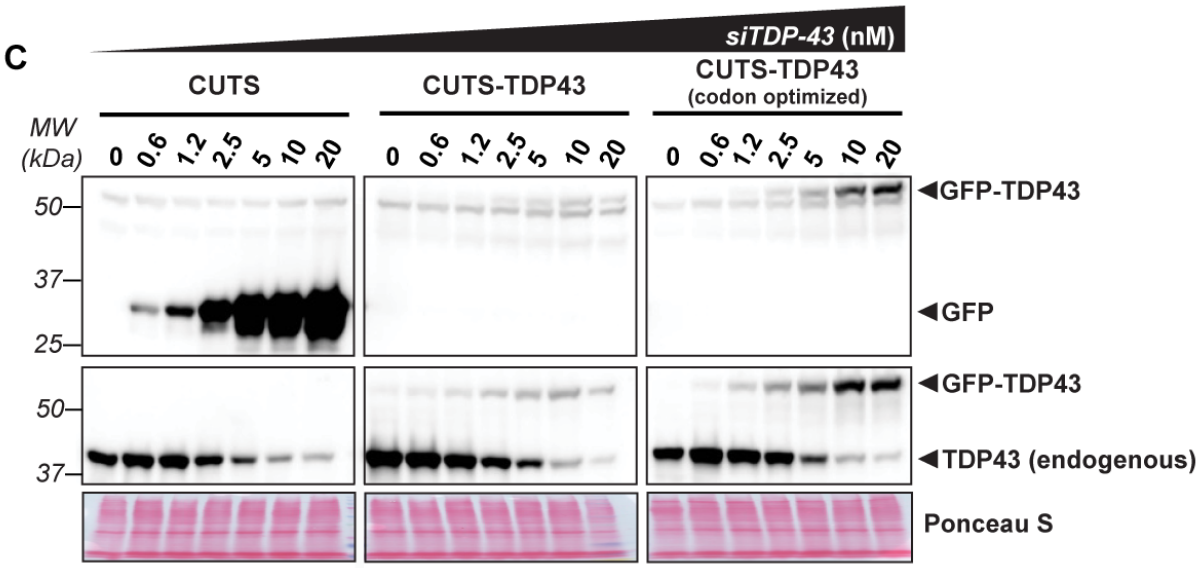
C
siTDP-43 (nM)
CUTS
CUTS-TDP43
CUTS-TDP43
(codon optimized)
MW
(kDa)
0
0.6
1.2
2.5
5
10
20
50
37
25
GFP-TDP43
GFP
TDP43 (endogenous)
Ponceau S

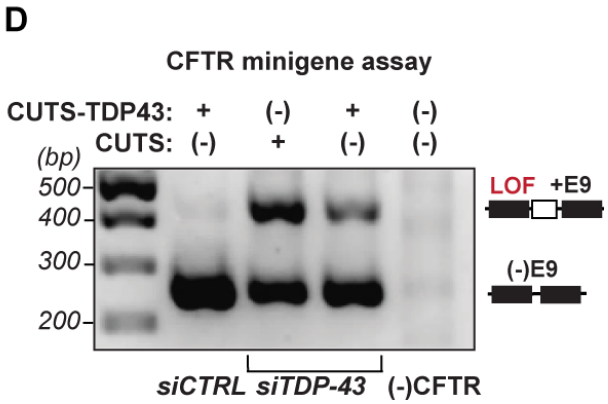
D
CFTR minigene assay
CUTS-TDP43: + (-) + (-)
CUTS: (-) + (-) (-)
(bp)
500
400
300
200
LOF +E9
(-)E9
siCTRL siTDP-43 (-)CFTR

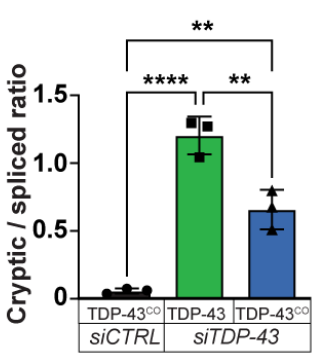
E
Cryptic / spliced ratio
1.5
1.0
0.5
0
**
****
**
TDP-43CO
TDP-43
TDP-43CO
siCTRL
siTDP-43

346

347 ***Figure 4: CUTS functions as an autoregulatory controller of TDP-43 expression.***
348 ***(A)*** *Schematic of CUTS as an autoregulatory controller of TDP-43 expression (CUTS-TDP43).*
349 ***(B-C)*** *TDP-43 siRNA (siTDP-43) dose-response curve in stable polyclonal HEK cells expressing*
350 *CUTS, CUTS-TDP43, or CUTS-TDP-43^{CO} (codon optimized). The codon-optimized variation*
351 *allows for continued expression during siTDP-43 treatment. HEK cells expressing the CUTS,*
352 *CUTS-TDP-43 and CUTS-TDP-43^{CO} were reverse transfected with control siRNA (siCTRL) or*
353 *siTDP-43 in a dose-response curve (0.6nM-20nM) in a doxycycline (1000ng/ml) supplement*
354 *media for 72hr. Cells were then used for live imaging or protein analysis. (B) Live imaging of the*
355 *CUTS variants. (C) Immunoblot assay of GFP and TDP-43. Ponceau S is shown as a loading*
356 *control.* ***(D-E)*** *CFTR minigene assay in stable CUTS or CUTS-TDP-43^{CO} expressing HEK cells.*
357 *Cells were induced with doxycycline (1000 ng/mL) for 24 h before transfection with the CFTR*
358 *minigene. Following an additional 24h of expression, cells were transfected with 20nM siCTRL or*
359 *siTDP-43. Cells were harvested 48 h following siRNA transfection for RNA extraction and RT-*
360 *PCR analysis. (D) PCR agarose gel of CFTR minigene. (E) PCR analysis of the ratio between*
361 *the CFTR cryptic exon inclusion and the correctly spliced product from CFTR as shown in (D).*
362 *Statistical significance was determined by One-Way ANOVA and Tukey Post-hoc (**, $p < 0.01$;*
363 *****, $p < 0.0001$). Green = GFP; red = mCherry. Scale bar = 100 μm. N=3 biological replicates.*

364 To test this, we created a new polyclonal stable line in HEK293 cells (CUTS-TDP43) by
365 replacing the 3xNLS in the original CUTS cassette with the *TARDBP* ORF fused to a GFP reporter
366 (Figure 4A). However, as our siTDP-43 targets the sequence within the coding region, CUTS-
367 TDP43 was also knocked down upon siRNA transfection, shown by a generalized decreased
368 mCherry signal (Figure 4B). Therefore, we designed a codon-optimized CUTS-TDP43^{CO} that is
369 not targeted by siTDP-43 (Figure 4B). Live imaging analyses showed that CUTS GFP signal
370 demonstrated a steady increase in expression in response to increasing doses of siTDP-43;
371 however, the GFP signal from CUTS-TDP43^{CO} remained undetectable (Figure 4B). WB analysis
372 further demonstrated successful TDP-43 rescue under endogenous TDP-43 KD, as shown by the
373 increasing exogenous TDP-43 observed following decreases in endogenous TDP-43 (Figure 4C).
374 The amount of total TDP-43 appeared to remain consistent throughout the increasing siTDP-43
375 doses, indicating tight regulation of the rescue parameters. To further confirm whether CUTS-
376 TDP43^{CO} could rescue TDP-43 splicing functionality, we performed a *CFTR* minigene assay
377 (Ayala et al., 2006; Buratti and Baralle, 2001). The expression of CUTS-TDP43^{SO} demonstrated
378 partial, yet significant rescue of cryptic exon 9 splicing in *CFTR* minigene, supporting its controlled
379 efficacy in rescuing splicing LOF (Figure 4D-4E). Taken together, these data indicate that CUTS
380 can autoregulate a TDP-43 payload to physiological levels in response to TDP-43 knockdown.

381 **Modeling CUTS system in neurons**

382 TDP-43 pathology primarily affects neurons; therefore, we adapted the CUTS system for use
383 in human neuronal models. In the original design, CUTS expression was driven by a Tet-On 3G
384 element under the control of the human phosphoglycerate kinase (hPGK) promoter. While hPGK
385 is generally considered a ubiquitous and stable promoter that drives moderate gene expression
386 and performs well in mitotic cells such as HEK293 and HeLa, several studies have reported
387 reduced activity or silencing of PGK-driven transgenes during neuronal differentiation(Xia et al.,
388 2007). To overcome this limitation, we developed an improved version of CUTS in which the Tet-
389 On 3G element is driven by the human synapsin I (hSYN1) promoter, providing more stable and
390 neuron-specific expression. In this optimized construct, we also replaced mCherry with mScarlet
391 to enhance fluorescence intensity and improve the dynamic range of detection. To test the
392 performance of this updated system, we generated stable human neuroblastoma BE(2)-C cell
393 lines expressing CUTS and examined mScarlett and GFP expression under 50 nM of siTDP-43
394 treatment in 10-day neuron-differentiated stages (Figure 5A-C). We observed robust and
395 inducible CUTS activation following siTDP-43 treatment in differentiated neurons, as shown by
396 GFP mean intensity in MAP-2 positive cells (Figure 5A-D, S4A). Furthermore, TDP-43
397 immunostaining demonstrated that cells with reduced TDP-43 protein levels corresponded to
398 GFP-positive cells (Figure 5B).

399 To validate CUTS performance in another human neuronal model, we generated the CUTS
400 human ReN primary neural cells. Stable CUTS-ReN cell lines were generated using a synapsin-
401 driven Tet3G doxycycline-inducible promoter. CUTS-ReN cells were differentiated for three
402 weeks prior to siTDP-43 treatment with increasing concentrations (25–100nM). Live-cell imaging
403 was performed to monitor mScarlet and GFP signals and revealed nuclear GFP in cells with as
404 little as 25 nM TDP-43 siRNA (Figure S4B). Using 100nM siRNA transfection,
405 immunofluorescence analysis of MAP2 and TDP-43 revealed GFP-positive neurons that
406 concurrently showed reduced nuclear TDP-43 levels (Figure 5D; white dotted lines indicate
407 nuclear GFP). Importantly, these GFP-positive cells were negative for the astrocytic marker GFAP
408 (Figure S4C), confirming neuronal specificity of the CUTS response.

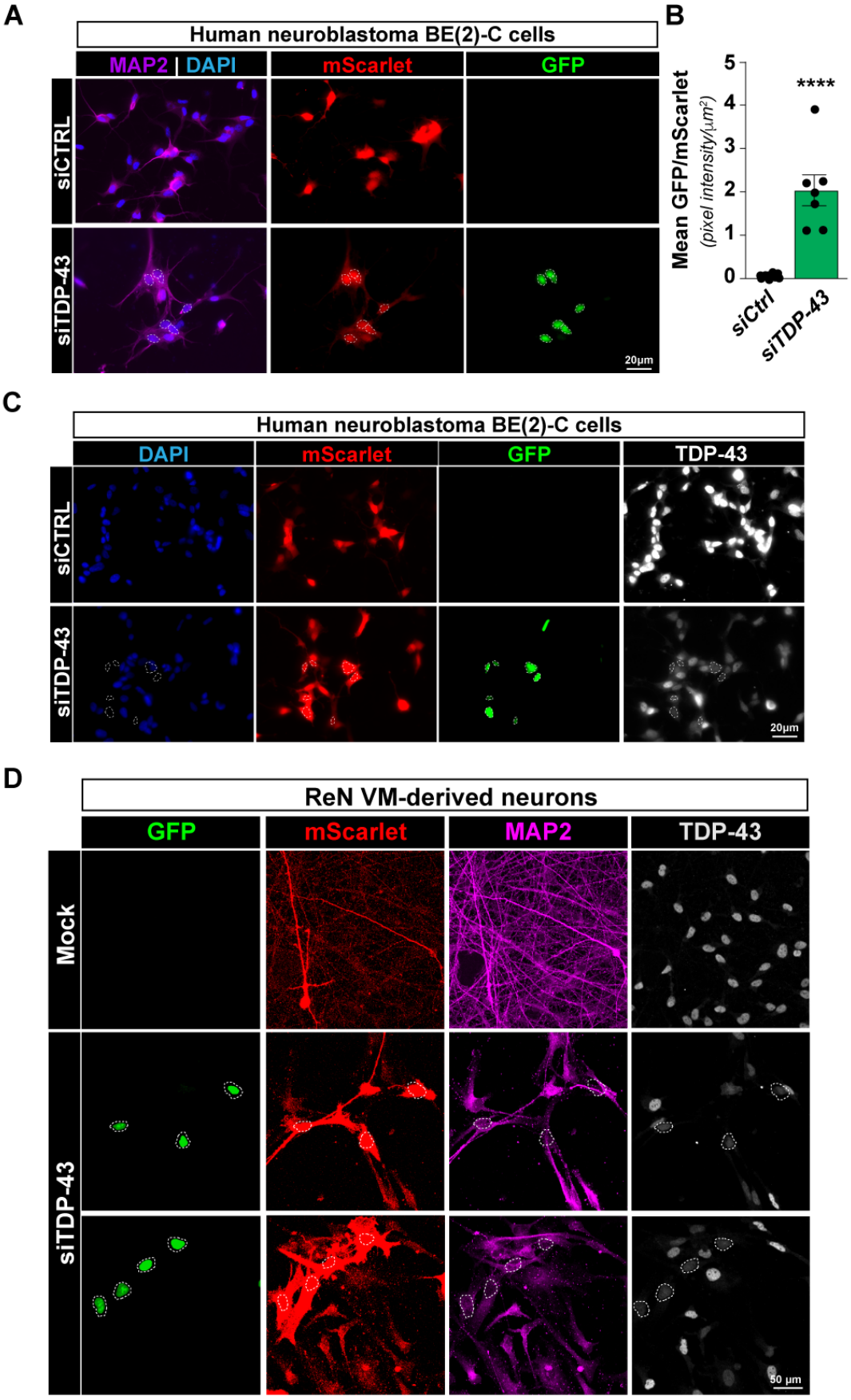
A
Human neuroblastoma BE(2)-C cells
MAP2 | DAPI
mScarlet
GFP
siCTRL
siTDP-43
20µm
B
Mean GFP/mScarlet
(pixel intensity/µm²)
5
4
3
2
1
0
****
siCtrl
siTDP-43
C
Human neuroblastoma BE(2)-C cells
DAPI
mScarlet
GFP
TDP-43
siCTRL
siTDP-43
20µm
D
ReN VM-derived neurons
GFP
mScarlet
MAP2
TDP-43
Mock
siTDP-43
50 µm

409

410 ***Figure 5: CUTS is activated in human neuronal models in response to TDP-43 LOF. (A)***
411 *Representative immunofluorescence images of MAP-2 (magenta), mScarlet, and GFP from*
412 *CUTS-expressing BE2C neuron-differentiated cells treated with siCtrl or siTDP-43 (50 nM). Scale*
413 *bar = 20 μM.* ***(B)*** *Mean GFP/mScarlet pixel intensity ratios from (A).* ***(C)*** *Representative*
414 *immunofluorescence images of TDP-43 (greyscale) and mScarlet-GFP signal from CUTS-*
415 *expressing BE(2)-C neuron-differentiated cells show reduced TDP-43 expression following siRNA*
416 *treatment. Fluorescence intensity quantification shows a 61.9 +/- 9.6 percent knockdown.*
417 *Scalebar = 20 μM.* ***(D)*** *Representative immunofluorescence images of MAP-2 (magenta),*
418 *TDP-43 (grey), mScarlet, and GFP from CUTS-expressing ReN differentiated neurons with 100*
419 *nM siRNA TDP-43. Nuclear GFP signals are indicated with a white dotted circle. Scalebar = 50*
420 *μM. Non-parametric Kolmogorov-Smirnov T-test (****, $p < 0.0001$).*

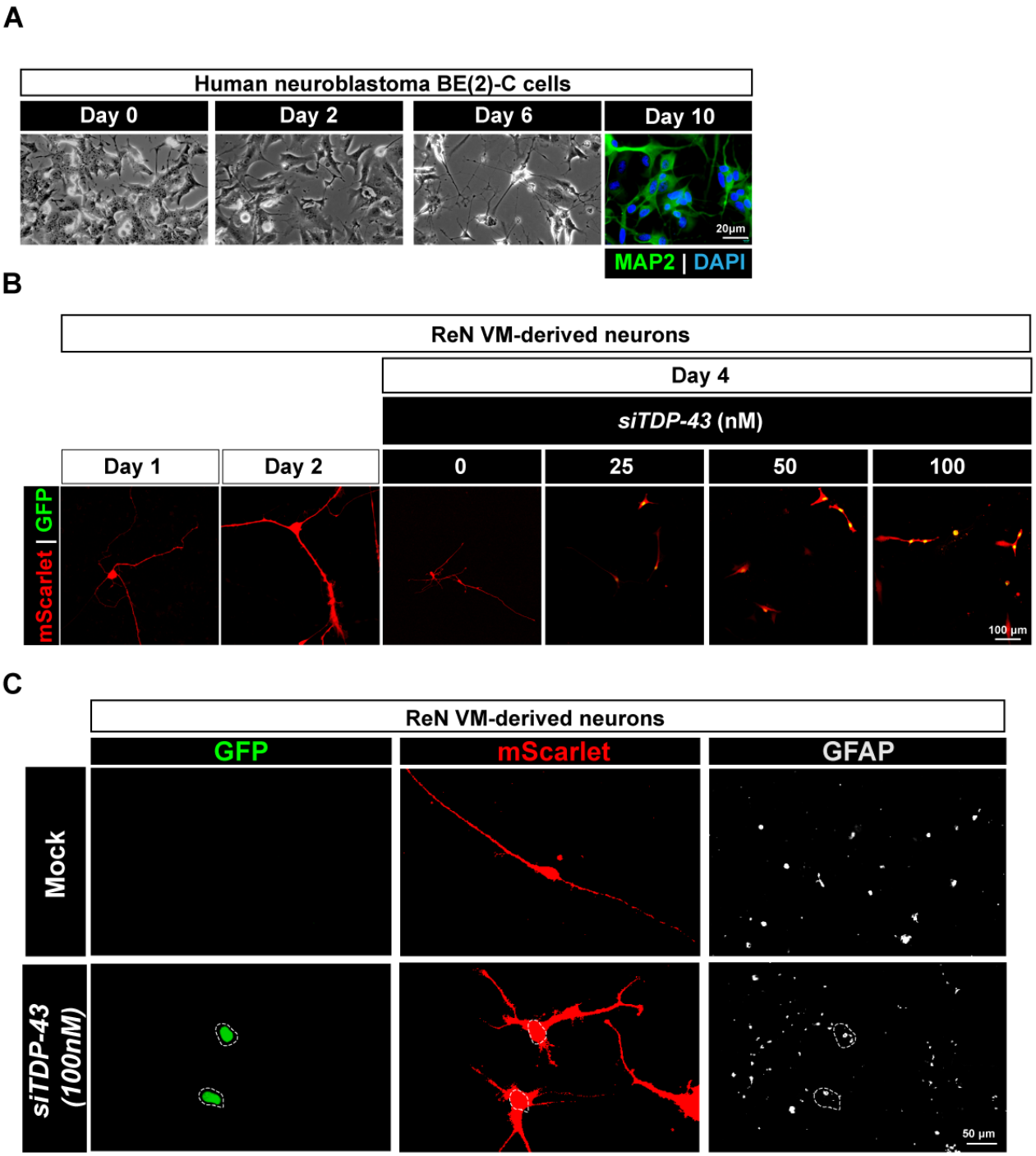

Supplementary Figure 4: CUTS activity in differentiated BE2C and ReN Cells. ***(A)*** *Representative bright-field images of BE2C differentiation from day 0 to day 6, after 10 days of differentiation, immunofluorescent staining was performed again MAP-2. Nuclei are indicated with a white dotted circle. Scalebar = 20 µM.* ***(B)*** *Representative mScarlet and GFP signal from live imagining of differentiated ReN cells expressing CUTS 2 days before siTDP-43 knockdown*

427 *and after 96 h of siRNA treatment at different siTDP-43 doses. Scalebar = 100 μM.* ***(C)***
428 *Representative immunofluorescent imaging of CUTS system in differentiated ReN VM cells*
429 *stained for GFAP (Greyscale). Nuclei are indicated with a white dotted circle. Scalebar = 50 μM.*

430

431 **Discussion**

432 We developed and characterized the CUTS system, a novel approach to detect TDP-43
433 LOF. The CUTS system utilizes TDP-43-dependent CE events to correlate the level of TDP-43
434 LOF directly with the expression of a GFP reporting gene. By combining the CFTR-TS and
435 UNC13A-TS, our findings demonstrate that the CUTS system provides an optimal balance of
436 sensitivity and accuracy. This was evidenced by the ability of CUTS to detect modest levels of
437 TDP-43 LOF, as shown by the dose-responsive increase in the expression of the reporter gene,
438 GFP, under various siTDP-43 concentrations (Figure 2). Furthermore, our results suggest that
439 CUTS can effectively discern TDP-43 LOF induced by pathological phase transitions or
440 mislocalization due to TDP-43 mutant or stressor, a critical aspect in the context of
441 neurodegenerative diseases containing TDP-43 pathology, such as ALS and FTLD. The CUTS
442 system's potential for application in gene-replacement therapies was also highlighted, offering a
443 promising avenue for autoregulated rescue of TDP-43 function, which is critical for avoiding the
444 deleterious effects of TDP-43 overexpression.

445 This tool findings enables for the significant advancement in the capacity to detect TDP-
446 43 LOF using biosensor assays across diverse experimental settings and through multiple
447 analytical methods. Previously, the *CFTR* minigene assay has been the predominant approach
448 for detecting TDP-43 LOF (Ayala et al., 2006; Buratti and Baralle, 2001; Cohen et al., 2015;
449 Conicella et al., 2020; Jiang et al., 2017; Schmidt et al., 2019). However, this approach is
450 associated with several limitations, all of which are effectively addressed by utilizing the CUTS
451 system. The first advantage of the CUTS system is its ability to detect TDP-43 LOF in real-time
452 through live-imaging analysis. Unlike *CFTR* minigene assays, which typically necessitate
453 endpoint experimental analysis, CUTS facilitates continuous monitoring, eliminating the need for
454 multiple fixed time points. Additionally, CUTS can be seamlessly integrated with various analytical
455 methods, including RT-qPCR (at the RNA level), WB analysis (at the protein level), live imaging
456 (for real-time assessment), and immunofluorescence imaging (to correlate with relevant markers).
457 While not evaluated in this study, it is conceivable that CUTS could be adapted for use with flow

458 cytometry-based techniques, leveraging GFP-positive cells as an output for analysis, as
459 previously demonstrated with a *CFTR*-modified sensor.

460 In addition to the expanded array of analytical methods offered by CUTS compared to
461 *CFTR* minigene assays, we anticipate that the CUTS system will exhibit superior sensitivity and
462 accuracy. This is supported by the comparison of CUTS with the CFTR-TS or UNC13A-TS
463 cassette (Figure 1), underscoring the potential of CUTS to outperform single minigene-based
464 approaches in TDP-43 LOF detection. Recent work characterizing other CE biosensors indicates
465 that CUTS exhibits comparable or, in some assays, enhanced sensitivity (Wilkins et al., 2024).
466 The expression of the GFP reporter in CUTS achieved up to 118,224-fold increase upon TDP-43
467 knockdown, compared to *ADNP2* (< 5-fold)(Zhang et al., 2024); TDP-REGv1 (<20-fold); and
468 TDP-REGv2 (<300-fold)(Wilkins et al., 2024). We also show that CUTS can detect ultra-low levels
469 of TDP-43 knockdown (increasing > 7-fold), below the WB or RT-qPCR detection limit.
470 Furthermore, CUTS exhibits a robust log-linear relationship to siRNA doses, making it suitable for
471 quantitative purposes.

472 The CUTS system outperformed traditional Western blot and transcript-based assays by
473 detecting as little as 1-2% TDP-43 knockdown, which was below the threshold of conventional
474 protein detection methods. This ultra-sensitivity aligns with recent evidence showing that even
475 subtle reductions in TDP-43 can disrupt splicing homeostasis and induce cryptic exon inclusion
476 in physiological targets such as *HDGFL2*, *ARHGAP32*, and *ACBD3* (Brown et al., 2022; Ma et al.,
477 2023; Fratta et al., 2018). The linear correlation between siTDP-43 dose and CUTS reporter
478 output underscores its predictive potential for quantifying graded LOF states. Importantly, the
479 observation that *HDGFL2* cryptic exon inclusion occurs at lower TDP-43 depletion levels supports
480 previous reports identifying it as one of the earliest and most sensitive markers of TDP-43
481 dysfunction (Humphrey et al., 2020; Seddighi et al., 2023). Thus, CUTS represents a robust and
482 scalable platform to detect and model early TDP-43-dependent splicing alterations.

483 Due to its success using *in vitro* models, we anticipate that CUTS might similarly be used
484 *in vivo* when coupled with disease models. Integrating the CUTS system with *in vitro* or *in vivo*
485 disease models enables the evaluation of the model's fidelity in recapitulating TDP-43 LOF
486 phenotypes. Such assessments are crucial for selecting appropriate models that faithfully
487 replicate the desired study context. Furthermore, coupling the CUTS system with TDP-43 models
488 presents a valuable approach for diverse screening studies. For example, CUTS can be
489 leveraged for high-throughput drug screening and CRISPR screening methodologies. Such
490 approaches hold promise for uncovering critical insights into cell-specific disease mechanisms,

491 identifying pivotal disease modifiers, and delineating potential therapeutic genetic targets
492 (Aldewachi et al., 2021; Bock et al., 2022).

493 A significant advantage of the CUTS system lies in its capacity to deliver precisely
494 regulated gene therapy for rescuing TDP-43 LOF. This study illustrates this capability by placing
495 a functional TDP-43 transcript downstream of the CUTS regulatory elements. The system's self-
496 regulating ability enhances its safety profile as a gene therapy approach, ensuring gene
497 expression occurs only when necessary and exclusively in cells lacking TDP-43 function.
498 Furthermore, this system can be expanded by substituting the TDP-43 transcript with other
499 genetic modifiers of disease, such as antibodies and PROTACs (Pozzi et al., 2019; Tseng et al.,
500 2023), or genes with established therapeutic potential, including heat shock proteins (HSPs) or
501 heterogeneous nuclear ribonucleoproteins (hnRNPs) (Koike et al., 2023; Lu et al., 2022; Yu et al.,
502 2021). This adaptability holds promise for achieving safe therapeutic outcomes without the need
503 for direct TDP-43 expression.

504

505 **Methods:**

506 **Generation of plasmids**

507 The CUTS sequence, plasmid, and map were originally generated in this study. The CFTR-TS,
508 UNC13A-TS, CUTS, DNA sequences were designed *in silico* and *de novo* synthesized by
509 Genewiz. These sequences were assembled into Tet3G vector between EcoRI and NotI with
510 NEBuilder HiFi DNA Assembly Master Mix (NEB, E2621L) following the manufacturer's protocol.
511 For CUTS:hSNY1 construction hSYN1 promoter and mScarlet DNA fragment were generated in
512 GenScript and TRE3G promoter was cut from CUTS plasmid by using ClaI and AfeI. After gel
513 recovery (D4001, ZYMO research) these sequences were assembled into Tet3G vector
514 containing CUTS sequence between PPuMI and XmaI with NEBuilder HiFi DNA Assembly Master
515 Mix (NEB, E2621L) following the manufacturer's protocol. Transform mix to competent cell
516 (C2987H, NEB) for the following ampicillin selection. Recombined plasmid was extracted by
517 QIAprep Spin Miniprep Kit (27104, QIAGEN) and confirmed by whole-plasmid sequencing. The
518 full DNA sequence for CUTS, CFTR-TS, UNC13A-TS and CUTS:hSNY1 can be found in Table
519 S1.

520 The CFTR minigene assay plasmid (pTB-CFTR-A455E) was a kind gift from Dr. Yuna Ayala.

521 The exogenous TDP-43 plasmids were constructed in a pCMV backbone by linking a 3xFlag-
522 APEX2 protein (Addgene #164622) (Bonet-Ponce et al., 2020) to TDP-43 coding sequences with
523 WT, cyto, 5FL, or cyto 5FL modifications (Mann et al., 2019).

524 The codon-optimized *TARDBP* coding sequence (Table S1) was synthesized by IDT and
525 assembled downstream of the GFP sequence of CUTS with NEBuilder HiFi DNA Assembly
526 Master Mix.

527 All the primers were synthesized by IDT. All plasmids were verified using whole-plasmid
528 sequencing via Oxford Nanopore, provided by Plasmidsaurus.

529

530 **Cell culture and transfection**

531 Human Embryonic Kidney 293 (HEK293) cells (female genotype, acquired from the American
532 Type Culture Collection (ATCC)) and HeLa TDP-43 knock-out (KO) cells (a kind gift from Dr.
533 Shawn M Ferguson) (Roczniak-Ferguson and Ferguson, 2019) were cultivated in Dulbecco's
534 Modified Eagle Medium high glucose, pyruvate (DMEM, Thermo Fisher Scientific, 10-313-039)
535 supplemented with 10% HyClone Bovine Growth Serum (Cytiva HyClon, SH3054103HI) and 1X
536 GlutaMAX (Thermo Fisher Scientific, 10-313-039). Cells were incubated at 37°C in a 5% CO2
537 atmosphere with high humidity. For transfection assays, cells were plated on collagen-coated
538 coverslips or dishes (50 µg/mL, GIBCO) and transfected with designated DNA quantities using
539 Lipofectamine 3000 (Thermo Scientific, L3000015) following the provider's protocol. BE(2)-C
540 neuroblastoma cells were maintained in DMEM/F12 (Gibco; Dulbecco's Modified Eagle
541 Medium/Nutrient Mixture F-12 with GlutaMAX™) supplemented with 10% FBS and cultured until
542 reaching 80–90% confluence. Neuronal differentiation was induced with 10 µM retinoic acid and
543 50 ng/mL BDNF for 10 days, as described previously (Targett et al., 2024). ReN VM cells were
544 maintained in proliferation medium consisting of DMEM/F12, B27 supplement, hEGF (20 ng/mL),
545 bFGF (20 ng/mL), and heparin (2 ng/mL) on Matrigel-coated plates. Once cultures reached ~90%
546 confluence, the medium was replaced with differentiation medium (DMEM/F12, B27, and 2 ng/mL
547 heparin) and cells were differentiated for 3 weeks. Full medium changes were performed every
548 other day during the first week, followed by half-medium changes every 4 days thereafter.

549

550 **Stable cell line generation via PiggyBac transposition**

551 For stable cell line creation, HEK293 or BE(2)-C neuroblastoma cells were pre-plated on 6-well
552 plates and transfected at approximately 70% confluence with 2.5 µg of PiggyBac plasmids
553 encoding CUTS, CFTR-TS, UNC13A-TS, and CUTS-TDP43 for HEKs cells or CUTS:hSNY1 for
554 BE(2)-C alongside with 0.5 µg of the Super PiggyBac Transposase Expressing plasmid
555 (PB200PA-1) using Lipofectamine 3000, according to the manufacturer's guidelines. A
556 transfection control without transposase was included. Following a 48-hour post-transfection
557 period, cells were selected with puromycin (Sigma, P8833) at 5 µg/mL, with media changes every
558 two days. Selection resulted in control cell death within approximately 5 days, while surviving
559 populations were expanded and maintained in reduced puromycin concentrations (2.5 µg/mL) to
560 establish stable lines. Expression of the transgenes was confirmed by immunofluorescence
561 staining and Western blot analysis. ReN VM neuronal precursor cells were electroporated using
562 the 4D-Nucleofector system (Lonza). Cells were subcultured two days before nucleofection to
563 reach ~80% confluence. At confluence, 7.5×10^5 cells were collected, centrifuged, and
564 resuspended in SF buffer (Lonza) containing 0.4 µg of PiggyBac plasmid encoding a
565 CUTS:hSNY1, which is human synapsin driving the Tet-On 3G transactivator gene to activate
566 CUTS expression upon doxycycline treatment, and 0.1 µg PiggyBac transposase plasmid.
567 Electroporation was performed in 16-well Nucleocuvette strips using the CM-137 program.
568 Following a 48-hour post-transfection period, cells were selected with puromycin (Sigma, P8833)
569 at 1 µg/mL, with media changes every two days. Selected CUTS:hSYN1 ReN VM neuronal
570 polyclonal precursor cells were differentiated for 3 weeks. Expression of the CUTS was confirmed
571 in CUTS:hSNY1 ReN VM neurons by live imaging and immunofluorescent staining following
572 treatment with 1000 ng/ml of Doxycycline for 5 days.

573

574 **Cellular stressor treatment**

575 Sodium arsenite ($NaAsO_2$) was prepared in fresh culture medium to a final concentration of 250
576 µM and applied to cells by complete medium exchange. For recovery, cells were washed once
577 with fresh medium and subsequently incubated in recovery medium for 5 hours.

578

579 **SDS-PAGE and Western blot**

580 For protein analysis, cells were lysed directly on the plate using fresh and pre-chilled Urea-RIPA
581 buffer: 2M fresh urea in 1XRIPA buffer (Boston Bioproducts, BP-115X), supplemented with 1%
582 protease inhibitor cocktail (Sigma, P8340) and sonicated. Protein concentrations were quantified
583 using the Pierce BCA Protein Assay Kit (Thermo Scientific, 23227). Proteins were resolved by
584 SDS-PAGE and transferred to nitrocellulose membranes for WB analysis. Membranes were
585 blocked and probed with primary antibodies: mouse-anti-GFP (Santa Cruz, sc-9996, 1:200),
586 mouse-anti-α-tubulin (Sigma, T5168, 1:1000), rabbit-anti-TDP-43 (Proteintech, 10782-2-AP,
587 1:2500), and rabbit-anti-mCherry (Cell Signaling, 43590, 1:1000), followed by HRP-conjugated
588 secondary antibodies: donkey-anti-mouse (JacksonImmunoResearch 715035151, 1:5000) or
589 donkey-anti-rabbit (JacksonImmunoResearch 711035152, 1:5000). Detection was achieved
590 using Western Lightning ECL Pro (Revvity, NEL1201001EA) or Supersignal West Femto
591 Maximum Sensitivity Chemiluminescent Substrate (Thermo Scientific, 34095) in an Amersham
592 ImageQuant 800 GxP biomolecular imager system (Amersham, 29653452).

593

594 **Fluorescence microscopy**

595 Confocal imaging was performed on a Nikon A1 laser-scanning microscope using either a 60X oil
596 immersion or a 10X/20X objective for live-cell observations. A Tokai HIT stage-top incubator
597 maintained the required environmental conditions. Representative images were chosen from at
598 least two independent experiments with a minimum of three biological replicates each. For live
599 imaging quantification, we measured the mean GFP signal intensity for each experimental
600 condition. The values were then averaged, and the results were used to calculate and plot the
601 fold change. For immunofluorescent imaging, we first created maximum intensity projection
602 images. We then applied masks to the GFP, mCherry/mScarlet, and Hoechst signals. By
603 overlapping the GFP and mCherry/mScarlet signals, we identified the number of GFP-positive
604 cells. Similarly, by overlapping the mCherry/mScarlet signal with the Hoechst mask, we identified
605 the CUTS-expressing cells. We then calculated a ratio of GFP-positive cells to CUTS-expressing
606 cells, plotted as a percentage of GFP-positive cells using the Nikon NIS software. Neuron-
607 differentiated BE(2)-C cells were stained for MAP2 (Millipore Cat# A5622, 1:500), TDP-43
608 (Proteintech, 10782-2-AP, 1:500) and Hoechst (1:10,000) and imaged using an Olympus IX71
609 inverted microscope equipped with 40X objective, a DP80 camera, and Olympus cellSens
610 software. Fluorescence intensity ratios were calculated across multiple image fields using ImageJ
611 FIJI.

612

613 **siRNA**

614 All siRNA treatments were performed as described using RNAiMAX (Thermo Scientific,
615 13778150) per manufacturers protocols. All siRNA experiments in CUTS:hSNY1 ReN VM
616 neurons were performed with RNAiMAX reagent and siRNA 48 h after Doxycycline treatment
617 (1000 ng/ml). Quantification occurred and quantified after 120 hr post RNAi treatment (168 hr post
618 Doxycycline treatment). Reverse transfections of siRNA were conducted using RNAiMAX reagent
619 adhering to the supplier's protocol. To knockdown TDP-43, the following siRNAs were used: ON-
620 TARGETplus SMARTpool siRNA against *TARDBP* (Dharmaco, L-012394-00-0005) and
621 siGENOME non-Targeting siRNA for control (Dharmaco, D-001206-13-05).

622

623 **RNA extraction, RT-PCR, and qPCR**

624 The RT-PCR or RT-qPCR was conducted with cDNA diluted 10-fold. For RT-PCR assay, CFTR
625 cryptic exon region was amplified with the following primer pair: P690-F (5'-
626 CAACTTCAAGCTCCTAAGCCACTGCCTGC) and P691-
627 R(5'TAGGATCCGGTCACCAGGAAGTTGGTTAAATCA). CUTS' cryptic exon region was
628 amplified with the following primer pair: CUTS-CE-F (5'-ATCCCGGCCCTGGATCCG) and CUTS-
629 CE-R (5'-GTCAGCTTGCCGTAGGTGGC). Endogenous cryptic exons including *LRP8*,
630 *EPB41L4A*, *ARHGAP32*, *ACBD3* and *HDGFL2* were amplified with the following primer pair:
631 LRP8-CE-F(5'-GGACGAGTTCCAGTGTGGG) and LRP8-CE-R(5'
632 GAAATCTGCGGGGACCCT); EPB41L4A-CE F (5'AGTCACCTTACAAAACAGAAGTCACA) and
633 EPB41L4A-CE-R(5'-ACATATGCACACACACTCTCACA); ARHGAP32-CE-F
634 (5'GGAGGAAGCATTTTGGAGGTTTCTA) and ARHGAP32-CE-R (5'-
635 CAGCCAAATGCACAGCGAAT); ACBD3-CE-F (5'-ACAGTATCCAGGGAACTACGAA) and
636 ACBD3-CE-R (5'-GCTTCCAGAGAAAGTACCTGTTGC); HDGFL2-CE-F (5'-
637 AAGACGCCTGCGCTAAAGAT) and HDGFL2-CE-R(5'-GCTTCCCTCCCTTCTGATGC). TDP-
638 43 and 18s were amplified using the following primers *RPS18*_FW (5'-
639 GCAGAATCCACGCCAGTACA) and RPS18_REV (5'-TTC ACGGAGCTTGTTGTCCA); *huTDP-*
640 *43*_FW (5'-TCATCCCCAAGCCATTCAGG) and REV (5'- TGC TTA GGT TCG GCA TTG GA).
641 PCR products were separated by agarose gel electrophoresis, and the bands were visualized
642 with Amersham ImageQuant 800 GxP biomolecular imager system.

643 For RT-qPCR assay, SsoAdvanced™ Universal SYBR Green Supermix (Biorad, 1725272) was
644 used following the supplier's protocol on a CFX96 Touch Real-Time PCR Detection System
645 (Biorad). Three technical replicates were included for each sample with the following program:
646 95°C for 30 s, 40 cycles of 95°C for 15 s and 60°C for 20 s. CUTS-CE-F (5'-
647 ATCCCGGCCCTGGATCCG) and CUTS-CE-R (5'-GTCAGCTTGCCGTAGGTGGC) were used
648 to quantify normal CUTS transcript. CUTS-J-F (5'-TCCGGCGAGGGATTTGGG) and CUTS-J-R
649 (5'-CCCCACCTAGACCCATCTCTCC) were primers targeting the cryptic exon junctions to
650 quantify cryptic exon-specific CUTS transcripts. Relative quantification of CUTS cryptic exon was
651 determined by the ΔCt value of CUTS-J normalized to CUTS-CE.

652 **Statistical analysis**

653 Statistical significance was evaluated using GraphPad Prism 9 software, and specific tests used
654 for each experiment are outlined in the respective figure legends.

655 **Authorship contributions**

656 LX, JM, and CAB share equal contributions and authorship. LX and BTH conceptualized the study.
657 LX, JM, and CAB were responsible for data curation, data analysis, conceptualizing and
658 performing the described methodologies, compiling and generating data, and writing the original
659 draft. JX assisted with data analyses and experimental optimization. SB and CTC contributed to
660 experimental design and analysis of the neuronal BE(2)-C studies and edited the manuscript, with
661 SB additionally constructing the stable BE(2)-C lines, conducting the experiments and collecting
662 data. CJD conceptualized the approach, funded the research, and prepared the final manuscript.

663 **Acknowledgments**

664 We thank Dr. Yuna Ayala, Ph.D. (St. Louis University School of Medicine), for kindly providing the
665 CFTR minigene plasmids. We thank Dr. Shawn M Ferguson, Ph.D. (Yale University School of
666 Medicine) for kindly providing the TARDBP$^{-/-}$ HeLa cell lines used in this study. We thank Olivia
667 R. Shapiro and Jocelyn C. Mauna (Donnelly Lab, University of Pittsburgh School of Medicine) for
668 their kind assistance and helpful discussions. This work was supported by funds to C.J.D. by the
669 LiveLikeLou Fund at the Pittsburgh Foundation and grants from NIH (R01NS105756,
670 R01NS127187) and R21AG075814 to C.T.C.

671

672 **Conflict of Interest Statement**

673 CJD is a consultant for Korro Bio. A provisional patent has been filed for the CUTS1 biosensor.

674

675

676 **Supplementary Table 1. Information of DNA sequence**

Domains of the sequence	Sequence
1. UNC13A-TS mCherry Linker-T2A HBA1_exon2 HBA1_intron 2 HBA1_exon3 UNC13A_modified_CE UNC13A_intron20 Linker-T2A EGFP 3XNLS	ATGGTGAGCAAGGGCGAGGAGGATAACATGGCCATCATCAAGG AGTTCATGCGCTTCAAGGTGCACATGGAGGGCTCCGTGAACGG CCACGAGTTCGAGATCGAGGGCGAGGGCGAGGGCCGCCCCTA CGAGGGCACCCAGACCGCCAAGCTGAAGGTGACCAAGGGTGG CCCCCTGCCCTTCGCCTGGGACATCCTGTCCCCTCAGTTCATGT ACGGCTCCAAGGCCTACGTGAAGCACCCCGCCGACATCCCCGA CTACTTGAAGCTGTCCTTCCCCGAGGGCTTCAAGTGGGAGCGC GTGATGAACTTCGAGGACGGCGGCGTGGTGACCGTGACCCAGG ACTCCTCCCTGCAGGACGGCGAGTTCATCTACAAGGTGAAGCTG CGCGGCACCAACTTCCCCTCCGACGGCCCCGTAATGCAGAAGA AGACCATGGGCTGGGAGGCCTCCTCCGAGCGGATGTACCCCGA GGACGGCGCCCTGAAGGGCGAGATCAAGCAGAGGCTGAAGCT GAAGGACGGCGGCCACTACGACGCTGAGGTCAAGACCACCTAC AAGGCCAAGAAGCCCGTGCAGCTGCCCGGCGCCTACAACGTCA ACATCAAGTTGGACATCACCTCCCACAACGAGGACTACACCATC GTGGAACAGTACGAACGCGCCGAGGGCCGCCACTCCACCGGC GGCATGGACGAGCTGTACAAGGGAGGTGGGGGATCTGGTGAG GGCAGAGGCAGTCTGCTGACATGCGGTGACGTGGAAGAGAATC CCGGCCCTGGATCCGGCCCGGTCAACTTCAAGGTGAGCGGCGG GCCGGGAGCGATCTGGGTCGAGGGGCGAGATGGCGCCTTCCT CGCAGGGCAGAGGATCACGCGGGTTGCGGGAGGTGTAGCGCA GGCGGCGGCTGCGGGCCTGGGCCCTCGGCCCCACTGACCCTC TTCTCTGCACAGCTCCTAAGCCACTGCCTGCTGGTGACCTCTGC CTGGGTTTCCTGGAAAGAACTCTTATCCCCAGGAACTAGTTTGTT GAATAAATGCTGGTGTGAATGTGAATGGATGATTGAACAGATGA ATGAGTGTGATGAGTATGATAAAAGCATGGATGGAGAGATGGGT GAGTACATGGATGGATAGATGGATGAGTTGGTGGGTAGATTCGT GGCTAGATGGATGATGGATGGATGGATGGATGGATGGATGGAT GGACAGATGGATGGATATATGATTGAACTATTGAAAGTATAGATG TATGGATGGGTGAATTTGGGGGTAATTGTTAGATGATGGATGTG GATGGTTGTGAGTGGCTGGTGGACAGACGAAAAATGGATGGGT GGATAAATTGATGGGTGGATGGATGGTTGGTTGTATGAAAGAAT GAATGATTGGGTAGATAAAAGAGTAGATGAATGAATTAATGAATA AACAGGCAGATGGATGATGTAAGCTGCCCCAGACCCTGGGACC TCTGACCCCCGGCGACCCCTTGCACTCTCCATGAGCCCTTTCCT

	TTTTTTTCCTCAGGTCTAGGTGGGGGATCTGGTGAGGGCAGAGG CAGTCTGCTGACATGCGGTGACGTGGAAGAGAATCCCGGCCCT TCTAGAAGCAAGGGCGAGGAGCTGTTCACCGGGGTGGTGCCCA TCCTGGTCGAGCTGGACGGCGACGTAAACGGCCACAAGTTCAG CGTGTCCGGCGAGGGCGAGGGCGATGCCACCTACGGCAAGCT GACCCTGAAGTTCATCTGCACCACCGGCAAGCTGCCCGTGCCC TGGCCCACCCTCGTGACCACCCTGACCTACGGCGTGCAGTGCT TCAGCCGCTACCCCGACCACATGAAGCAGCACGACTTCTTCAAG TCCGCCATGCCCGAAGGCTACGTCCAGGAGCGCACCATCTTCTT CAAGGACGACGGCAACTACAAGACCCGCGCCGAGGTGAAGTTC GAGGGCGACACCCTGGTGAACCGCATCGAGCTGAAGGGCATCG ACTTCAAGGAGGACGGCAACATCCTGGGGCACAAGCTGGAGTA CAACTACAACAGCCACAACGTCTATATCATGGCCGACAAGCAGA AGAACGGCATCAAGGTGAACTTCAAGATCCGCCACAACATCGAG GACGGCAGCGTGCAGCTCGCCGACCACTACCAGCAGAACACCC CCATCGGCGACGGCCCCGTGCTGCTGCCCGACAACCACTACCT GAGCACCCAGTCCGCCCTGAGCAAAGACCCCAACGAGAAGCGC GATCACATGGTCCTGCTGGAGTTCGTGACCGCCGCCGGGATCA CTCTCGGCATGGACGAGCTGTACAAGCTGCAGAGCAGGGCCGA CCCCAAGAAGAAGAGGAAGGTGGACCCCAAGAAGAAGAGGAAG GTGGACCCCAAGAAGAAGAGGAAGGTGTGA
2. CFTR-TS mCherry Linker-T2A CFTR_intron 8 CFTR_modified_exon9 CFTR_intron 9 Linker-T2A EGFP 3XNLS	ATGGTGAGCAAGGGCGAGGAGGATAACATGGCCATCATCAAGG AGTTCATGCGCTTCAAGGTGCACATGGAGGGCTCCGTGAACGG CCACGAGTTCGAGATCGAGGGCGAGGGCGAGGGCCGCCCCTA CGAGGGCACCCAGACCGCCAAGCTGAAGGTGACCAAGGGTGG CCCCCTGCCCTTCGCCTGGGACATCCTGTCCCCTCAGTTCATGT ACGGCTCCAAGGCCTACGTGAAGCACCCCGCCGACATCCCCGA CTACTTGAAGCTGTCCTTCCCCGAGGGCTTCAAGTGGGAGCGC GTGATGAACTTCGAGGACGGCGGCGTGGTGACCGTGACCCAGG ACTCCTCCCTGCAGGACGGCGAGTTCATCTACAAGGTGAAGCTG CGCGGCACCAACTTCCCCTCCGACGGCCCCGTAATGCAGAAGA AGACCATGGGCTGGGAGGCCTCCTCCGAGCGGATGTACCCCGA GGACGGCGCCCTGAAGGGCGAGATCAAGCAGAGGCTGAAGCT GAAGGACGGCGGCCACTACGACGCTGAGGTCAAGACCACCTAC AAGGCCAAGAAGCCCGTGCAGCTGCCCGGCGCCTACAACGTCA ACATCAAGTTGGACATCACCTCCCACAACGAGGACTACACCATC GTGGAACAGTACGAACGCGCCGAGGGCCGCCACTCCACCGGC GGCATGGACGAGCTGTACAAGGGAGGTGGGGGATCTGGTGAG GGCAGAGGCAGTCTGCTGACATGCGGTGACGTGGAAGAGAATC

	CCGGCCCTGGATCCGGCGAGGTGAGTATGGTACATAAAACAAG CATCTATTGAAAATATCTGACAAACTCATCTTTTATTTTTGATGTG TGTGTGTGTGTGTGTGTGTGTGTTTTTTTTTAACAGGGATTTGGG GAATTATTTGAGAAAGCAAAACAAAACAATAACAATAGAAAAACT TCTAATGGTGATGACAGCCAAGATAGAAAGAGGACAGTTGTTGG AGGTTGCTGGATCCACTGGAGCAGGCAAGGTAGTTCTTTTGTTC TTCACTATTAAGAACTTAATTTGGTGCCCATGTCTCTTTTTTTTTC TAGTTTGTAGTGCTGGAAGGTATTTTTGGAGAAATTCTTACATGA GCATTAGGAGAATGTATGGGTGTAGTGTCTTGTATAATAGAAATT GTTCCACTGATAATTTACTCTAGTTTTTTATTTCCTCATATTATTTT CAGTGGCTTTTTCTTCCACATCTTTATATTTTGCACCACATTCAAC ACTGTATCTTGCACATGGCGAGCATATGGTCGATGATGTAAGCT GCCCCAGACCCTGGGACCTCTGACCCCCGGCGACCCCTTGCAC TCTCCATGAGCCCTTTCCTTTTTTTTCCTCAGGTCTAGGTGGGGG ATCTGGTGAGGGCAGAGGCAGTCTGCTGACATGCGGTGACGTG GAAGAGAATCCCGGCCCTTCTAGAAGCAAGGGCGAGGAGCTGT TCACCGGGGTGGTGCCCATCCTGGTCGAGCTGGACGGCGACGT AAACGGCCACAAGTTCAGCGTGTCCGGCGAGGGCGAGGGCGAT GCCACCTACGGCAAGCTGACCCTGAAGTTCATCTGCACCACCG GCAAGCTGCCCGTGCCCTGGCCCACCCTCGTGACCACCCTGAC CTACGGCGTGCAGTGCTTCAGCCGCTACCCCGACCACATGAAG CAGCACGACTTCTTCAAGTCCGCCATGCCCGAAGGCTACGTCCA GGAGCGCACCATCTTCTTCAAGGACGACGGCAACTACAAGACCC GCGCCGAGGTGAAGTTCGAGGGCGACACCCTGGTGAACCGCAT CGAGCTGAAGGGCATCGACTTCAAGGAGGACGGCAACATCCTG GGGCACAAGCTGGAGTACAACTACAACAGCCACAACGTCTATAT CATGGCCGACAAGCAGAAGAACGGCATCAAGGTGAACTTCAAGA TCCGCCACAACATCGAGGACGGCAGCGTGCAGCTCGCCGACCA CTACCAGCAGAACACCCCCATCGGCGACGGCCCCGTGCTGCTG CCCGACAACCACTACCTGAGCACCCAGTCCGCCCTGAGCAAAG ACCCCAACGAGAAGCGCGATCACATGGTCCTGCTGGAGTTCGT GACCGCCGCCGGGATCACTCTCGGCATGGACGAGCTGTACAAG CTGCAGAGCAGGGCCGACCCCAAGAAGAAGAGGAAGGTGGACC CCAAGAAGAAGAGGAAGGTGGACCCCAAGAAGAAGAGGAAGGT GTGA
3. CUTS mCherry Linker-T2A	ATGGTGAGCAAGGGCGAGGAGGATAACATGGCCATCATCAAGG AGTTCATGCGCTTCAAGGTGCACATGGAGGGCTCCGTGAACGG CCACGAGTTCGAGATCGAGGGCGAGGGCGAGGGCCGCCCCTA CGAGGGCACCCAGACCGCCAAGCTGAAGGTGACCAAGGGTGG

CFTR_intron 8 CFTR_modified_exon9 UNC13A_modified_CE UNC13A_intron20 Linker-T2A EGFP 3XNLS	CCCCCTGCCCTTCGCCTGGGACATCCTGTCCCCTCAGTTCATGT ACGGCTCCAAGGCCTACGTGAAGCACCCCGCCGACATCCCCGA CTACTTGAAGCTGTCCTTCCCCGAGGGCTTCAAGTGGGAGCGC GTGATGAACTTCGAGGACGGCGGCGTGGTGACCGTGACCCAGG ACTCCTCCCTGCAGGACGGCGAGTTCATCTACAAGGTGAAGCTG CGCGGCACCAACTTCCCCTCCGACGGCCCCGTAATGCAGAAGA AGACCATGGGCTGGGAGGCCTCCTCCGAGCGGATGTACCCCGA GGACGGCGCCCTGAAGGGCGAGATCAAGCAGAGGCTGAAGCT GAAGGACGGCGGCCACTACGACGCTGAGGTCAAGACCACCTAC AAGGCCAAGAAGCCCGTGCAGCTGCCCGGCGCCTACAACGTCA ACATCAAGTTGGACATCACCTCCCACAACGAGGACTACACCATC GTGGAACAGTACGAACGCGCCGAGGGCCGCCACTCCACCGGC GGCATGGACGAGCTGTACAAGGGAGGTGGGGGATCTGGTGAG GGCAGAGGCAGTCTGCTGACATGCGGTGACGTGGAAGAGAATC CCGGCCCTGGATCCGGCGAGGTGAGTATGGTACATAAAACAAG CATCTATTGAAAATATCTGACAAACTCATCTTTTATTTTTGATGTG TGTGTGTGTGTGTGTGTGTGTGTTTTTTTTTAACAGGGATTTGGG GAATTATTTGAGAAAGCAAAACAAAACAATAACAATAGAAAAACT TCTAATGGTGATGACAGCACTGCCTGGGTTTCCTGGAAAGAACT CTTATCCCCAGGAACTAGTTTGTTGAATAAATGCTGGTGTGAATG TGAATGGATGATTGAACAGATGAATGAGTGTGATGAGTATGATAA AAGCATGGATGGAGAGATGGGTGAGTACATGGATGGATAGATG GATGAGTTGGTGGGTAGATTCGTGGCTAGATGGATGATGGATGG ATGGATGGATGGATGGATGGATGGACAGATGGATGGATATATGA TTGAACTATTGAAAGTATAGATGTATGGATGGGTGAATTTGGGG GTAATTGTTAGATGATGGATGTGGATGGTTGTGAGTGGCTGGTG GACAGACGAAAAATGGATGGGTGGATAAATTGATGGGTGGATGG ATGGTTGGTTGTATGAAAGAATGAATGATTGGGTAGATAAAAGAG TAGATGAATGAATTAATGAATAAACAGGCAGATGGATGATGTAAG CTGCCCCAGACCCTGGGACCTCTGACCCCCGGCGACCCCTTGC ACTCTCCATGAGCCCTTTCCTTTTTTTTCCTCAGGTCTAGGTGGG GGATCTGGTGAGGGCAGAGGCAGTCTGCTGACATGCGGTGACG TGGAAGAGAATCCCGGCCCTTCTAGAAGCAAGGGCGAGGAGCT GTTCACCGGGGTGGTGCCCATCCTGGTCGAGCTGGACGGCGAC GTAAACGGCCACAAGTTCAGCGTGTCCGGCGAGGGCGAGGGC GATGCCACCTACGGCAAGCTGACCCTGAAGTTCATCTGCACCAC CGGCAAGCTGCCCGTGCCCTGGCCCACCCTCGTGACCACCCTG ACCTACGGCGTGCAGTGCTTCAGCCGCTACCCCGACCACATGA AGCAGCACGACTTCTTCAAGTCCGCCATGCCCGAAGGCTACGTC CAGGAGCGCACCATCTTCTTCAAGGACGACGGCAACTACAAGAC

	CCGCGCCGAGGTGAAGTTCGAGGGCGACACCCTGGTGAACCGC ATCGAGCTGAAGGGCATCGACTTCAAGGAGGACGGCAACATCC TGGGGCACAAGCTGGAGTACAACTACAACAGCCACAACGTCTAT ATCATGGCCGACAAGCAGAAGAACGGCATCAAGGTGAACTTCAA GATCCGCCACAACATCGAGGACGGCAGCGTGCAGCTCGCCGAC CACTACCAGCAGAACACCCCCATCGGCGACGGCCCCGTGCTGC TGCCCGACAACCACTACCTGAGCACCCAGTCCGCCCTGAGCAA AGACCCCAACGAGAAGCGCGATCACATGGTCCTGCTGGAGTTC GTGACCGCCGCCGGGATCACTCTCGGCATGGACGAGCTGTACA AGCTGCAGAGCAGGGCCGACCCCAAGAAGAAGAGGAAGGTGGA CCCCAAGAAGAAGAGGAAGGTGGACCCCAAGAAGAAGAGGAAG GTGTGA
4. Codon-optimized TDP-43	ATGTCTGAATATATTCGGGTAACCGAAGATGAGAACGATGAACC AATCGAAATTCCAAGTGAAGACGACGGAACAGTCTTGCTCTCCA CAGTAACGGCGCAGTTTCCCGGTGCGTGCGGATTGAGATATCG CAACCCGGTGTCTCAGTGCATGCGAGGTGTAAGGTTGGTCGAA GGGATCCTGCACGCCCCCGATGCAGGCTGGGGTAACCTCGTGT ACGTGGTTAACTACCCGAAGGATAACAAGAGGAAAATGGATGAA ACCGATGCTAGTTCCGCCGTGAAGGTGAAACGAGCGGTTCAAAA AACTTCAGATCTTATAGTTCTGGGCCTCCCTTGGAAGACCACGG AACAGGATTTGAAAGAGTATTTTTCAACCTTTGGCGAGGTTCTCA TGGTGCAGGTTAAAAAAGATCTTAAAACCGGACACTCAAAAGGA TTTGGCTTCGTGAGGTTCACCGAGTACGAAACGCAGGTAAAAGT GATGTCACAGCGCCATATGATAGACGGACGGTGGTGCGATTGTA AGCTGCCCAATTCCAAGCAAAGCCAAGACGAGCCTCTGAGGAGT CGCAAAGTTTTCGTTGGACGCTGTACGGAAGACATGACTGAAGA TGAGCTTAGGGAGTTTTTTAGTCAGTATGGAGACGTTATGGATGT CTTTATCCCAAAACCGTTTCGGGCCTTCGCCTTTGTCACCTTTGC CGACGACCAGATCGCCCAGAGCTTGTGTGGCGAAGACCTGATA ATTAAAGGTATATCTGTCCATATCAGCAATGCGGAACCGAAACAC AACTCTAATCGACAGCTTGAGAGGTCAGGGAGGTTTGGGGGTAA CCCGGGTGGATTCGGTAACCAAGGGGGGTTCGGAAACTCCCGG GGCGGAGGAGCCGGATTGGGTAATAACCAGGGATCCAACATGG GCGGCGGGATGAACTTTGGTGCCTTCTCCATAAATCCTGCGATG ATGGCCGCAGCGCAAGCTGCCCTTCAGAGCTCCTGGGGTATGA TGGGGATGCTTGCTTCTCAGCAAAACCAATCCGGGCCCAGCGG CAACAATCAGAATCAAGGTAATATGCAGCGAGAACCGAACCAGG CCTTCGGAAGCGGGAATAATTCCTACTCAGGATCAAATAGTGGT GCAGCCATTGGCTGGGGCTCAGCGTCTAATGCAGGCTCAGGCA

	GTGGGTTTAATGGGGGCTTTGGGAGCTCCATGGACAGCAAGTC ATCAGGCTGGGGGTAA
5. CUTS hSYN1 mScarlet Linker-T2A CFTR_intron 8 CFTR_modifi ed_exon9 UNC13A_mo dified_CE	AGTGCAAGTGGGTTTTAGGACCAGGATGAGGCGGGGTGGGGGT GCCTACCTGACGACCGACCCCGACCCACTGGACAAGCACCCAA CCCCCATTCCCCAAATTGCGCATCCCCTATCAGAGAGGGGGAG GGGAAACAGGATGCGGCGAGGCGCGTGCGCACTGCCAGCTTCA GCACCGCGGACAGTGCCTTCGCCCCCGCCTGGCGGCGCGCGC CACCGCCGCCTCAGCACTGAAGGCGCGCTGACGTCACTCGCCG GTCCCCCGCAAACTCCCCTTCCCGGCCACCTTGGTCGCGTCCG CGCCGCCGCCGGCCCAGCCGGACCGCACCACGCGAGGCGCGA GATAGGGGGGCACGGGCGCGACCATCTGCGCTGCGGCGCCGG CGACTCAGCGCTGCCTCAGTCTGCGGTGGGCAGCGGAGGAGTC GTGTCGTGCCTGAGAGCGCAG

691 **References**

692 Aldewachi H, Al-Zidan RN, Conner MT, Salman MM. 2021. High-Throughput Screening
693 Platforms in the Discovery of Novel Drugs for Neurodegenerative Diseases. *Bioengineering*
694 *(Basel)* **8**. doi:10.3390/bioengineering8020030

695 Ayala YM, Pagani F, Baralle FE. 2006. TDP43 depletion rescues aberrant CFTR exon 9
696 skipping. *FEBS Lett* **580**:1339–1344. doi:10.1016/j.febslet.2006.01.052

697 Baughn MW, Melamed Z, López-Erauskin J, Beccari MS, Ling K, Zuberi A, Presa M, Gonzalo-
698 Gil E, Maimon R, Vazquez-Sanchez S, Chaturvedi S, Bravo-Hernández M, Taupin V, Moore
699 S, Artates JW, Acks E, Ndayambaje IS, Agra de Almeida Quadros AR, Jafar-Nejad P, Rigo F,
700 Bennett CF, Lutz C, Lagier-Tourenne C, Cleveland DW. 2023. Mechanism of STMN2 cryptic
701 splice-polyadenylation and its correction for TDP-43 proteinopathies. *Science* **379**:1140–
702 1149. doi:10.1126/science.abq5622

703 Bock C, Datlinger P, Chardon F, Coelho MA, Dong MB, Lawson KA, Lu T, Maroc L, Norman
704 TM, Song B, Stanley G, Chen S, Garnett M, Li W, Moffat J, Qi LS, Shapiro RS, Shendure J,
705 Weissman JS, Zhuang X. 2022. High-content CRISPR screening. *Nat Rev Methods Primers*
706 **2**. doi:10.1038/s43586-022-00098-7

707 Bonet-Ponce L, Beilina A, Williamson CD, Lindberg E, Kluss JH, Saez-Atienzar S, Landeck N,
708 Kumaran R, Mamais A, Bleck CKE, Li Y, Cookson MR. 2020. LRRK2 mediates tubulation and
709 vesicle sorting from lysosomes. *Sci Adv* **6**. doi:10.1126/sciadv.abb2454

710 Brown A-L, Wilkins OG, Keuss MJ, Kargbo-Hill SE, Zanovello M, Lee WC, Bampton A, Lee
711 FCY, Masino L, Qi YA, Bryce-Smith S, Gatt A, Hallegger M, Fagegaltier D, Phatnani H,
712 NYGC ALS Consortium, Newcombe J, Gustavsson EK, Seddighi S, Reyes JF, Coon SL,
713 Ramos D, Schiavo G, Fisher EMC, Raj T, Secrier M, Lashley T, Ule J, Buratti E, Humphrey J,
714 Ward ME, Fratta P. 2022. TDP-43 loss and ALS-risk SNPs drive mis-splicing and depletion of
715 UNC13A. *Nature* **603**:131–137. doi:10.1038/s41586-022-04436-3

716 Buratti E, Baralle FE. 2001. Characterization and functional implications of the RNA binding
717 properties of nuclear factor TDP-43, a novel splicing regulator of CFTR exon 9. *J Biol Chem*
718 **276**:36337–36343. doi:10.1074/jbc.M104236200

719 Cohen TJ, Hwang AW, Restrepo CR, Yuan C-X, Trojanowski JQ, Lee VMY. 2015. An
720 acetylation switch controls TDP-43 function and aggregation propensity. *Nat Commun*
721 **6**:5845. doi:10.1038/ncomms6845

722 Conicella AE, Dignon GL, Zerze GH, Schmidt HB, D'Ordine AM, Kim YC, Rohatgi R, Ayala YM,
723 Mittal J, Fawzi NL. 2020. TDP-43 α-helical structure tunes liquid-liquid phase separation and
724 function. *Proc Natl Acad Sci USA* **117**:5883–5894. doi:10.1073/pnas.1912055117

725 Elden AC, Kim H-J, Hart MP, Chen-Plotkin AS, Johnson BS, Fang X, Armakola M, Geser F,
726 Greene R, Lu MM, Padmanabhan A, Clay-Falcone D, McCluskey L, Elman L, Juhr D, Gruber
727 PJ, Rüb U, Auburger G, Trojanowski JQ, Lee VM-Y, Van Deerlin VM, Bonini NM, Gitler AD.
728 2010. Ataxin-2 intermediate-length polyglutamine expansions are associated with increased
729 risk for ALS. *Nature* **466**:1069–1075. doi:10.1038/nature09320

730 Estades Ayuso V, Pickles S, Todd T, Yue M, Jansen-West K, Song Y, González Bejarano J,
731 Rawlinson B, DeTure M, Graff-Radford NR, Boeve BF, Knopman DS, Petersen RC, Dickson
732 DW, Josephs KA, Petrucelli L, Prudencio M. 2023. TDP-43-regulated cryptic RNAs
733 accumulate in Alzheimer's disease brains. *Mol Neurodegener* **18**:57. doi:10.1186/s13024-
734 023-00646-z

735 Feldman EL, Goutman SA, Petri S, Mazzini L, Savelieff MG, Shaw PJ, Sobue G. 2022.
736 Amyotrophic lateral sclerosis. *Lancet* **400**:1363–1380. doi:10.1016/S0140-6736(22)01272-7

737 Huang W-P, Ellis BCS, Hodgson RE, Sanchez Avila A, Kumar V, Rayment J, Moll T,
738 Shelkovnikova TA. 2024. Stress-induced TDP-43 nuclear condensation causes splicing loss
739 of function and STMN2 depletion. *Cell Rep* **43**:114421. doi:10.1016/j.celrep.2024.114421

740 Hurtle BT, Xie L, Donnelly CJ. 2023. Disrupting pathologic phase transitions in
741 neurodegeneration. *J Clin Invest* **133**. doi:10.1172/JCI168549

742 Jiang L-L, Xue W, Hong J-Y, Zhang J-T, Li M-J, Yu S-N, He J-H, Hu H-Y. 2017. The N-terminal
743 dimerization is required for TDP-43 splicing activity. *Sci Rep* **7**:6196. doi:10.1038/s41598-017-
744 06263-3

745 Johnson BS, Snead D, Lee JJ, McCaffery JM, Shorter J, Gitler AD. 2009. TDP-43 is intrinsically
746 aggregation-prone, and amyotrophic lateral sclerosis-linked mutations accelerate aggregation
747 and increase toxicity. *J Biol Chem* **284**:20329–20339. doi:10.1074/jbc.M109.010264

748 Joseph BJ, Marshall KA, Harley P, Mann JR, Alessandrini F, Vanoye CG, Chi W, Prudencio M,
749 Simkin D, Kao T-T, Desai RR, Keuss MJ, Barattucci S, Zanovello M, Mehta PR, DeKeyser J-
750 M, Limone F, Lee J, Brown A-L, Leyton-Jaimes MF, Nash LA, Juan IGS, Aronica E, Wainger
751 BJ, Shah M, Goswami A, Shneider NA, Dickson DW, Burrone J, Zhang C, Wichterle H,
752 Petrucelli L, Watts JK, George AL, Fratta P, Eggan K, Kiskinis E. 2025. TDP-43-dependent
753 mis-splicing of KCNQ2 triggers intrinsic neuronal hyperexcitability in ALS/FTD. *Nat Neurosci*
754 **28**:2476–2492. doi:10.1038/s41593-025-02096-w

755 Keating SS, Bademosi AT, San Gil R, Walker AK. 2023. Aggregation-prone TDP-43 sequesters
756 and drives pathological transitions of free nuclear TDP-43. *Cell Mol Life Sci* **80**:95.
757 doi:10.1007/s00018-023-04739-2

758 Klim JR, Williams LA, Limone F, Guerra San Juan I, Davis-Dusenbery BN, Mordes DA, Burberry
759 A, Steinbaugh MJ, Gamage KK, Kirchner R, Moccia R, Cassel SH, Chen K, Wainger BJ,
760 Woolf CJ, Eggan K. 2019. ALS-implicated protein TDP-43 sustains levels of STMN2, a
761 mediator of motor neuron growth and repair. *Nat Neurosci* **22**:167–179. doi:10.1038/s41593-
762 018-0300-4

763 Koike Y, Pickles S, Estades Ayuso V, Jansen-West K, Qi YA, Li Z, Daughrity LM, Yue M, Zhang
764 Y-J, Cook CN, Dickson DW, Ward M, Petrucelli L, Prudencio M. 2023. TDP-43 and other
765 hnRNPs regulate cryptic exon inclusion of a key ALS/FTD risk gene, UNC13A. *PLoS Biol*
766 **21**:e3002028. doi:10.1371/journal.pbio.3002028

767 Kuo P-H, Doudeva LG, Wang Y-T, Shen C-KJ, Yuan HS. 2009. Structural insights into TDP-43
768 in nucleic-acid binding and domain interactions. *Nucleic Acids Res* **37**:1799–1808.
769 doi:10.1093/nar/gkp013

770 Ling JP, Pletnikova O, Troncoso JC, Wong PC. 2015. TDP-43 repression of nonconserved
771 cryptic exons is compromised in ALS-FTD. *Science* **349**:650–655.
772 doi:10.1126/science.aab0983

773 Ling S-C, Polymenidou M, Cleveland DW. 2013. Converging mechanisms in ALS and FTD:
774 disrupted RNA and protein homeostasis. *Neuron* **79**:416–438.
775 doi:10.1016/j.neuron.2013.07.033

776 Lukavsky PJ, Daujotyte D, Tollervey JR, Ule J, Stuani C, Buratti E, Baralle FE, Damberger FF,
777 Allain FH-T. 2013. Molecular basis of UG-rich RNA recognition by the human splicing factor
778 TDP-43. *Nat Struct Mol Biol* **20**:1443–1449. doi:10.1038/nsmb.2698

779 Lu S, Hu J, Arogundade OA, Goginashvili A, Vazquez-Sanchez S, Diedrich JK, Gu J, Blum J,
780 Oung S, Ye Q, Yu H, Ravits J, Liu C, Yates JR, Cleveland DW. 2022. Heat-shock chaperone
781 HSPB1 regulates cytoplasmic TDP-43 phase separation and liquid-to-gel transition. *Nat Cell*
782 *Biol* **24**:1378–1393. doi:10.1038/s41556-022-00988-8

783 Mann JR, Donnelly CJ. 2021. RNA modulates physiological and neuropathological protein
784 phase transitions. *Neuron* **109**:2663–2681. doi:10.1016/j.neuron.2021.06.023

785 Mann JR, Gleixner AM, Mauna JC, Gomes E, DeChellis-Marks MR, Needham PG, Copley KE,
786 Hurtle B, Portz B, Pyles NJ, Guo L, Calder CB, Wills ZP, Pandey UB, Kofler JK, Brodsky JL,
787 Thathiah A, Shorter J, Donnelly CJ. 2019. RNA Binding Antagonizes Neurotoxic Phase
788 Transitions of TDP-43. *Neuron* **102**:321-338.e8. doi:10.1016/j.neuron.2019.01.048

789 Ma XR, Prudencio M, Koike Y, Vatsavayai SC, Kim G, Harbinski F, Briner A, Rodriguez CM,
790 Guo C, Akiyama T, Schmidt HB, Cummings BB, Wyatt DW, Kurylo K, Miller G, Mekhoubad S,
791 Sallee N, Mekonnen G, Ganser L, Rubien JD, Jansen-West K, Cook CN, Pickles S,
792 Oskarsson B, Graff-Radford NR, Boeve BF, Knopman DS, Petersen RC, Dickson DW,
793 Shorter J, Myong S, Green EM, Seeley WW, Petrucelli L, Gitler AD. 2022. TDP-43 represses
794 cryptic exon inclusion in the FTD-ALS gene UNC13A. *Nature* **603**:124–130.
795 doi:10.1038/s41586-022-04424-7

796 McKee AC, Gavett BE, Stern RA, Nowinski CJ, Cantu RC, Kowall NW, Perl DP, Hedley-Whyte
797 ET, Price B, Sullivan C, Morin P, Lee H-S, Kubilus CA, Daneshvar DH, Wulff M, Budson AE.
798 2010. TDP-43 proteinopathy and motor neuron disease in chronic traumatic encephalopathy.
799 *J Neuropathol Exp Neurol* **69**:918–929. doi:10.1097/NEN.0b013e3181ee7d85

800 Mehta PR, Brown A-L, Ward ME, Fratta P. 2023. The era of cryptic exons: implications for ALS-
801 FTD. *Mol Neurodegener* **18**:16. doi:10.1186/s13024-023-00608-5

802 Melamed Z, López-Erauskin J, Baughn MW, Zhang O, Drenner K, Sun Y, Freyermuth F,
803 McMahon MA, Beccari MS, Artates JW, Ohkubo T, Rodriguez M, Lin N, Wu D, Bennett CF,
804 Rigo F, Da Cruz S, Ravits J, Lagier-Tourenne C, Cleveland DW. 2019. Premature
805 polyadenylation-mediated loss of stathmin-2 is a hallmark of TDP-43-dependent
806 neurodegeneration. *Nat Neurosci* **22**:180–190. doi:10.1038/s41593-018-0293-z

807 Nelson PT, Dickson DW, Trojanowski JQ, Jack CR, Boyle PA, Arfanakis K, Rademakers R,
808 Alafuzoff I, Attems J, Brayne C, Coyle-Gilchrist ITS, Chui HC, Fardo DW, Flanagan ME,
809 Halliday G, Hokkanen SRK, Hunter S, Jicha GA, Katsumata Y, Kawas CH, Keene CD,
810 Kovacs GG, Kukull WA, Levey AI, Makkinejad N, Montine TJ, Murayama S, Murray ME, Nag
811 S, Rissman RA, Seeley WW, Sperling RA, White CL, Yu L, Schneider JA. 2019. Limbic-
812 predominant age-related TDP-43 encephalopathy (LATE): consensus working group report.
813 *Brain* **142**:1503–1527. doi:10.1093/brain/awz099

814 Neumann M, Sampathu DM, Kwong LK, Truax AC, Micsenyi MC, Chou TT, Bruce J, Schuck T,
815 Grossman M, Clark CM, McCluskey LF, Miller BL, Masliah E, Mackenzie IR, Feldman H,
816 Feiden W, Kretzschmar HA, Trojanowski JQ, Lee VM-Y. 2006. Ubiquitinated TDP-43 in
817 frontotemporal lobar degeneration and amyotrophic lateral sclerosis. *Science* **314**:130–133.
818 doi:10.1126/science.1134108

819 Park S-K, Hong JY, Arslan F, Kanneganti V, Patel B, Tietsort A, Tank EMH, Li X, Barmada SJ,
820 Liebman SW. 2017. Overexpression of the essential Sis1 chaperone reduces TDP-43 effects
821 on toxicity and proteolysis. *PLoS Genet* **13**:e1006805. doi:10.1371/journal.pgen.1006805

822 Polymenidou M, Lagier-Tourenne C, Hutt KR, Huelga SC, Moran J, Liang TY, Ling S-C, Sun E,
823 Wancewicz E, Mazur C, Kordasiewicz H, Sedaghat Y, Donohue JP, Shiue L, Bennett CF, Yeo
824 GW, Cleveland DW. 2011. Long pre-mRNA depletion and RNA missplicing contribute to
825 neuronal vulnerability from loss of TDP-43. *Nat Neurosci* **14**:459–468. doi:10.1038/nn.2779

826 Pozzi S, Thammisetty SS, Codron P, Rahimian R, Plourde KV, Soucy G, Bareil C, Phaneuf D,
827 Kriz J, Gravel C, Julien J-P. 2019. Virus-mediated delivery of antibody targeting TAR DNA-
828 binding protein-43 mitigates associated neuropathology. *J Clin Invest* **129**:1581–1595.
829 doi:10.1172/JCI123931

830 Roczniak-Ferguson A, Ferguson SM. 2019. Pleiotropic requirements for human TDP-43 in the
831 regulation of cell and organelle homeostasis. *Life Sci Alliance* **2**. doi:10.26508/lsa.201900358

832 Schmidt HB, Barreau A, Rohatgi R. 2019. Phase separation-deficient TDP43 remains functional
833 in splicing. *Nat Commun* **10**:4890. doi:10.1038/s41467-019-12740-2

834 Shin JE, Geisler S, DiAntonio A. 2014. Dynamic regulation of SCG10 in regenerating axons
835 after injury. *Exp Neurol* **252**:1–11. doi:10.1016/j.expneurol.2013.11.007

836 Shin JE, Miller BR, Babetto E, Cho Y, Sasaki Y, Qayum S, Russler EV, Cavalli V, Milbrandt J,
837 DiAntonio A. 2012. SCG10 is a JNK target in the axonal degeneration pathway. *Proc Natl*
838 *Acad Sci USA* **109**:E3696-705. doi:10.1073/pnas.1216204109

839 Sun M, Bell W, LaClair KD, Ling JP, Han H, Kageyama Y, Pletnikova O, Troncoso JC, Wong
840 PC, Chen LL. 2017. Cryptic exon incorporation occurs in Alzheimer's brain lacking TDP-43
841 inclusion but exhibiting nuclear clearance of TDP-43. *Acta Neuropathol* **133**:923–931.
842 doi:10.1007/s00401-017-1701-2

843 Tremblay C, St-Amour I, Schneider J, Bennett DA, Calon F. 2011. Accumulation of transactive
844 response DNA binding protein 43 in mild cognitive impairment and Alzheimer disease. *J*
845 *Neuropathol Exp Neurol* **70**:788–798. doi:10.1097/NEN.0b013e31822c62cf

846 Tseng Y-L, Lu P-C, Lee C-C, He R-Y, Huang Y-A, Tseng Y-C, Cheng T-JR, Huang JJ-T, Fang
847 J-M. 2023. Degradation of neurodegenerative disease-associated TDP-43 aggregates and
848 oligomers via a proteolysis-targeting chimera. *J Biomed Sci* **30**:27. doi:10.1186/s12929-023-
849 00921-7

850 Varoqueaux F, Sigler A, Rhee J-S, Brose N, Enk C, Reim K, Rosenmund C. 2002. Total arrest
851 of spontaneous and evoked synaptic transmission but normal synaptogenesis in the absence
852 of Munc13-mediated vesicle priming. *Proc Natl Acad Sci USA* **99**:9037–9042.
853 doi:10.1073/pnas.122623799

854 Wilkins OG, Chien MZYJ, Wlaschin JJ, Barattucci S, Harley P, Mattedi F, Mehta PR, Pisliakova
855 M, Ryadnov E, Keuss MJ, Thompson D, Digby H, Knez L, Simkin RL, Diaz JA, Zanovello M,
856 Brown A-L, Darbey A, Karda R, Fisher EMC, Cunningham TJ, Le Pichon CE, Ule J, Fratta P.
857 2024. Creation of de novo cryptic splicing for ALS and FTD precision medicine. *Science*
858 **386**:61–69. doi:10.1126/science.adk2539

859 Willemse SW, Harley P, van Eijk RPA, Demaegd KC, Zelina P, Pasterkamp RJ, van Damme P,
860 Ingre C, van Rheenen W, Veldink JH, Kiernan MC, Al-Chalabi A, van den Berg LH, Fratta P,
861 van Es MA. 2023. UNC13A in amyotrophic lateral sclerosis: from genetic association to
862 therapeutic target. *J Neurol Neurosurg Psychiatr* **94**:649–656. doi:10.1136/jnnp-2022-330504

863 Xia X, Zhang Y, Zieth CR, Zhang S-C. 2007. Transgenes delivered by lentiviral vector are
864 suppressed in human embryonic stem cells in a promoter-dependent manner. *Stem Cells Dev*
865 **16**:167–176. doi:10.1089/scd.2006.0057

866 Yang C, Qiao T, Yu J, Wang H, Guo Y, Salameh J, Metterville J, Parsi S, Yusuf I, Brown RH,
867 Cai H, Xu Z. 2022. Low-level overexpression of wild type TDP-43 causes late-onset,
868 progressive neurodegeneration and paralysis in mice. *PLoS ONE* **17**:e0255710.
869 doi:10.1371/journal.pone.0255710

870 Yu H, Lu S, Gasior K, Singh D, Vazquez-Sanchez S, Tapia O, Toprani D, Beccari MS, Yates
871 JR, Da Cruz S, Newby JM, Lafarga M, Gladfelter AS, Villa E, Cleveland DW. 2021. HSP70
872 chaperones RNA-free TDP-43 into anisotropic intranuclear liquid spherical shells. *Science*
873 **371**. doi:10.1126/science.abb4309

874 Zhang X, Das T, Chao TF, Trinh V, Carmen-Orozco RP, Ling JP, Kalab P, Hayes LR. 2024.
875 Multivalent GU-rich oligonucleotides sequester TDP-43 in the nucleus by inducing high
876 molecular weight RNP complexes. *iScience* **27**:110109. doi:10.1016/j.isci.2024.110109